Tampere University

Aravind Ramesh

JAMMING DETECTION USING WAVELET TRANSFORMS

Faculty of Information
Technology and Communication
Sciences
Master of Science Thesis
May 2019

ABSTRACT

Aravind Ramesh : Jamming Detection using Wavelet Transforms
Master of Science Thesis
Tampere University
MSc. Tech in Electrical Engineering (Major: Wireless Communications)
May 2019

Modern Global Navigation Satellite Systems (GNSS), such as GPS and Galileo, play vital role in providing high precision navigation and positioning services for civilian and military applications. The high precision feature of these systems is compromised in the presence of interference, particularly intentional narrowband interference otherwise commonly known as jamming. To ensure the sustainability of high precision, removal of jamming components is necessary. In order to achieve successful elimination of jamming components, efficient detection and understanding of the nature of jamming signals are vital.

In practice, signals are finite in nature and vary over time. Mathematical tools such as Fourier transforms assume signals are infinite (periodic), thereby fail to capture accurate time-related information. To overcome this situation, a sophisticated technique that captures valuable information in both time and frequency domains is required. One such technique is the wavelet transform.

Wavelet transform involves successive scaling of fast decaying wavelike oscillations known as wavelets in time and shifting it along the duration of an incoming signal. This process results in either stretching or shrinking of wavelets. Stretched wavelet facilitates the extraction of slow variations in a signal and compressed wavelet facilitates the extraction of abrupt variations.

The conceived algorithm detects the presence of jamming signals, simultaneously capturing features such as frequency, bandwidth and duration. The operational capability of the algorithm was tested for GNSS signals operating in L1 frequency band (1575.42MHz) such as GPS L1 and Galileo E1. The parameters defined to measure the efficiency of the algorithm are detection probability (Pd) and false alarm probability (Pfa). Pd is estimated for different values of jammer to signal ratio (JSR) with fixed signal to noise ratio (SNR) and Pfa depends on the choice of detection threshold (T). T is chosen such that Pfa is as low as possible. The detector works better in low noise and high jammer power scenarios.

Keywords: Jamming, Wavelets, GPS, Galileo, SNR, JSR, L1

PREFACE

In this thesis, I have presented a technique to detect intentional interference using the concept of wavelet transform. The entire study is divided into four chapters. Chapter 1 contains short Introduction to the topic, chapter 2 talks about necessary theoretical background, chapter 3 discusses the simulation results and chapter 4 showcases the conclusions of the study.

I would like to thank Associate Prof. Elena Simona Lohan and Prof. Jari Nurmi for their valuable guidance, support and for giving me an opportunity to work on a rare and interesting topic with plenty of practical applications.

Tampere, 13 May 2019

Aravind Ramesh

LIST OF SYMBOLS AND ABBREVIATIONS

ADC	Analog to Digital Converter
AGC	Automatic Gain Control
BOC	Binary Offset Carrier
BPSK	Binary Phase Shift keying
CW	Continuous Wave
CWT	Continuous Wavelet Transform
D	Decision Metric
DWT	Discrete Wavelet Transform
GNSS	Global Navigation Satellite System
GPS	Global Positioning System
IF	Intermediate Frequency
JSR	Jammer to Signal Ratio
LO	Local Oscillator
MODWT	Maximum Overlap Discrete Wavelet Transform
SNR	Signal to Noise Ratio
T	Detection Threshold
$\Psi(t)$	Mother wavelet
a	CWT shifting factor
f	frequency (Hz)
f_0	Initial frequency
f_1	Final frequency
F_c	Centre frequency
F_e	Equivalent frequency
g[n]	Low pass filter function
h[n]	High pass filter function
r	rate of change of frequency
$r(t)$	Received signal
s	CWT scaling factor
v	DWT scaling and shifting parameter
ω	Angular frequency (rad/s)

LIST OF FIGURES

CONTENTS

1. INTRODUCTION

1.1 Objectives and Motivation

The primary objective of the thesis is to develop an efficient signal analysis algorithm to identify intentional interference components know as jamming, present in GNSS signals. Satellite systems are basically used for navigation and positioning purposes including sensitive military applications like missile guidance and radar tracking systems, which requires high precision and accurate service. Presence of jamming severely compromises the efficiency of such systems.

To ensure proper functionality of a satellite system, detection and elimination of jamming signal components are key requirements. Here, the focus of our study is localised to the detection part. Since signals in real life are finite in nature, efficient detection of jamming signals can be achieved with mathematical techniques that are well localised in both time and frequency domains. One such technique is based on wavelet transform.

Wavelet transform technique involves stretching and shrinking of fast decaying, short duration oscillations resulting in scales of different central frequencies and passing these various scaled oscillations along the duration of the signal to be analysed. This process extracts valuable information related to jamming signals such as frequency, magnitude and duration among other things. Depending on how the wavelets are scaled and shifted, wavelet transforms can be divides into types namely continuous wavelet transforms (CWT) and discrete wavelet transforms (DWT). CWT and DWT has its own virtues and vices.

The detection algorithm conceived based on the above approach results in vast number of factors known as wavelet coefficients. The size of the wavelet coefficients depends on variety of parameters including the duration of the received signal. In CWT, the down converted received signal is analysed with multiple wavelet scales each with specific centre frequency, which allows for better characterization of the signal of interest (In this case GNSS signals operating in L1 band). On the other hand, In DWT, the same signal is passes through a series of unique low pass and high pass filters resulting in approximation and detail coefficients. A variant of DWT known as maximum overlap discrete wavelet transform (MODWT) is used in our detection algorithm instead of conventional

DWT. MODWT works very similar to conventional DWT but with minor differences which better suits to our requirement in this study.

The efficiency of the algorithm is measured based on two parameters namely, detection probability (Pd) and false alarm probability (Pfa). Based on the results obtained, the detection algorithm conceived in this thesis works better in low noise and high jammer power scenarios.

1.2 State of the Art

In modern signal processing, time-frequency analysis-based techniques such as wavelet transform are being extensively used to study signals (data) that are well localized in time including communication signals plagued by interference. The advantages offered by wavelet transform compared to other mathematical tools such as Fourier transform makes it suitable for signal analysis including but not limited to interference detection and mitigation. Some of the complex set ups where wavelet transform is primarily used to identify interference are,

- power electronic systems affected by electromagnetic interference [2].
- Radio receivers designed to receive spread spectrum signals in the presence of narrow band intentional interference [14].
- Automotive civilian radars working close to each other (vulnerable to interference) [15].
- Frequency hop spread spectrum systems in the presence of narrow band interference [16].
- Synthetic Aperture Radar systems prone to narrow band interference [17].
- Microwave radiometry systems vulnerable to radio frequency interference [18].
- Electromyogram systems containing electrocardiogram signals (interference) [19].
- Electronic systems responsible for electromagnetic interference and noise in coal mines [20].

All these applications prove that effectiveness of wavelet transform in signal processing and analysis.

1.3 Author's Contribution

The following were the contributions made by the author in this thesis,

- Research on relevant theoretical framework and simulation studies.
- Development and simulation of the wavelet-based interference detection algorithm.
- Analysis of simulation results.
- Documentation of the entire work.

All accomplished under the guidance of associate professor. Elena-Simona Lohan and professor. Jari Nurmi.

The remaining part of the study is discussed in three chapters with chapter 2 presenting the theoretical backbone, chapter 3 presenting the simulation and analysis part and finally chapter 4 presenting the conclusions and future work.

2. THEORETICAL BACKGROUND

2.1. GNSS Signals

The signals transmitted by satellites operating in GNSS systems are called GNSS signals. Depending on wide variety of characteristics, there are different types of GNSS signals such as GPS, Galileo, GLONASS and BeiDou. These signals are transmitted at one or more frequencies in L band. In this study, we are interested in satellite signals transmitted in L1 (1575.42MHz) frequency band [12].

The main components of a GNSS signal are [12],

- *Ranging code or spreading sequence*: Binary sequence of 1's and 0's processed by a GNSS receiver to extract valuable information like time required by a GNSS signal to travel from satellite to receiver.
- *Navigation Data*: A message coded in binary form containing information on health of the satellite, satellite position and velocity, parameters related to satellite clock bias and other supporting information.
- *Carrier*: Radio frequency sinusoidal signal at a certain frequency.

In this study, the detection is algorithm is applied for GNSS signals operating in L1 frequency band such as,

1. *GPS L1 C/A*: The main components are, coarse/acquisition (C/A) code of length 1023 chips with a chipping rate of 1.023MHz, Navigation data with 50Hz data rate which are then combined based on X-OR logic and modulated onto the L1 carrier transmitting at 1575.42MHz using Binary Phase Shift keying (BPSK) Scheme. Figure 1 shows the main components of a GPS L1 C/A signal and figure 2 shows the transmitted signal on the L1 carrier.
2. *Galileo L1OS*: The main components are, spreading sequence of length 4092 bits with chipping rate of 1.023MHz, subcarrier, Binary Offset carrier (BOC) modulated code and navigation date transmitted on L1 frequency band at 1575.42MHz. The use of BOC enables to focus the power of the signal in certain regions of the frequency band. This technique reduces interference with other GNSS signals at the receiver. One other advantage of BOC modulation technique is its ability to split the original BPSK spectrum (GPS L1 C/A) into two symmetrical parts thereby leaving no power on the carrier. Binary offset carrier offers two design variables namely, subcarrier frequency (fs in MHz) and

spreading code rate (fc in Mchip/s) that allows to achieve this. Figure 3 depicts the comparison of original and BOC modulated BPSK spectrums.

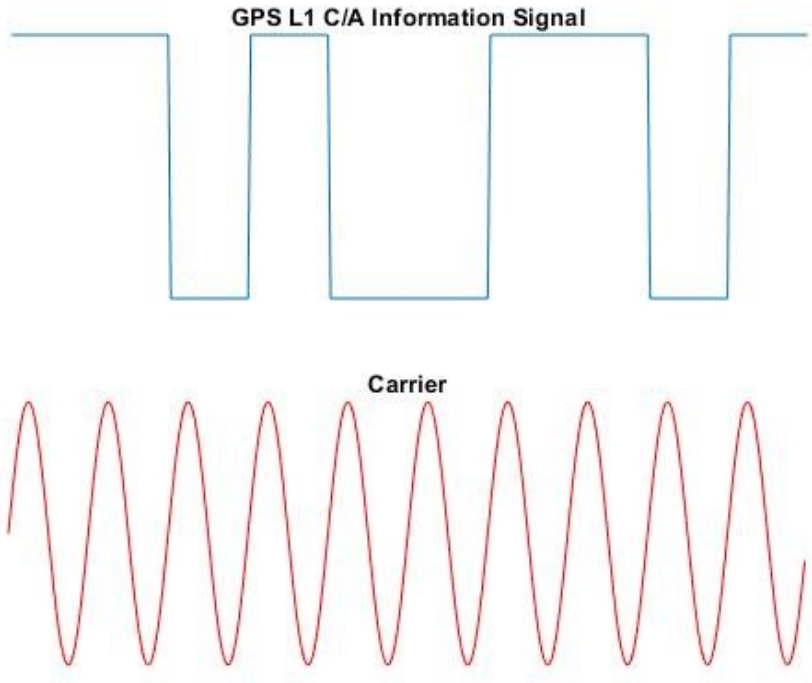

Figure 1. Components of GPS L1 C/A satellite signal (Information and Carrier signals).

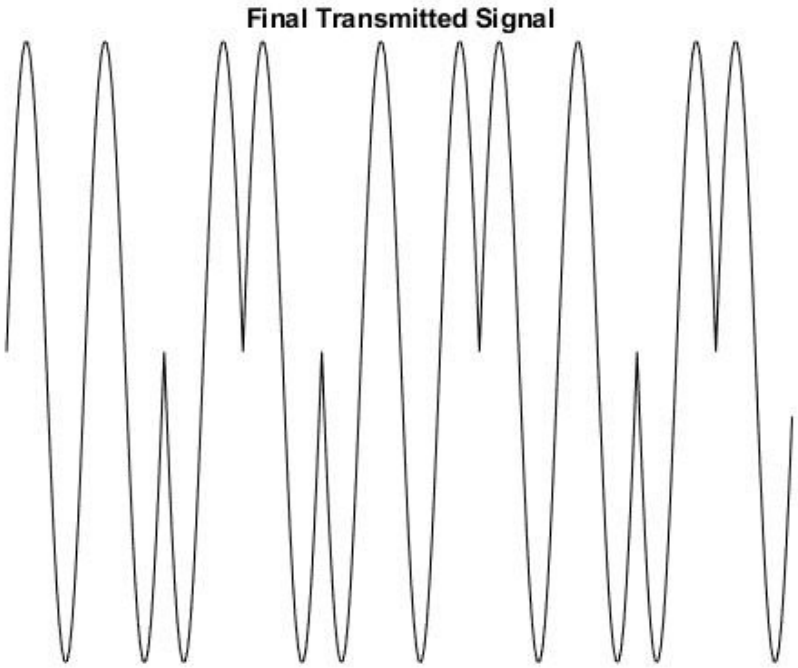

Figure 2. Transmitted GPS L1 C/A signal.

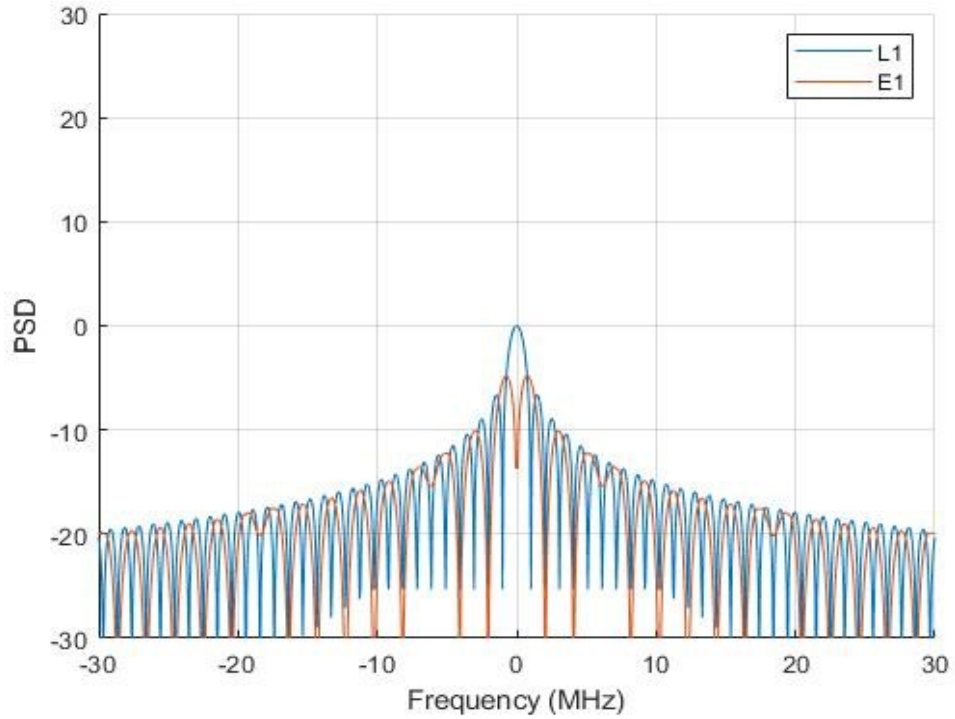

Figure 3. MATLAB simulation of the spectrum of GPS C/A and Galileo BOC (1,1) on L1 frequency band. PSD is measured in dB.

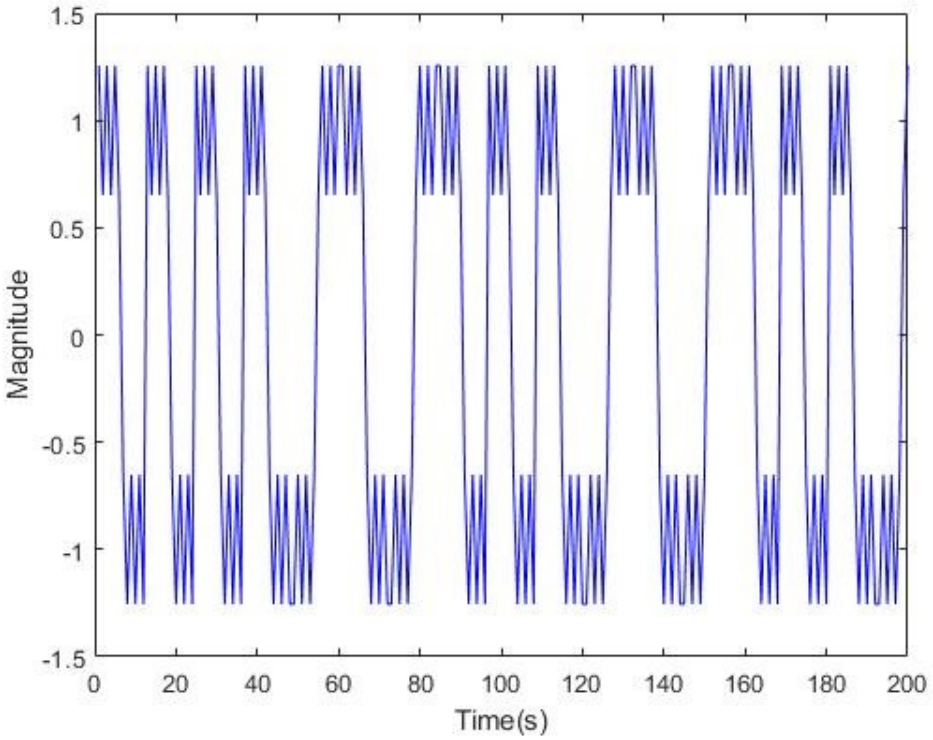

Figure 4. MATLAB simulation of Galileo L1 signal before modulating onto the carrier.

2.2 GNSS receiver front end

The front end of a GNSS receiver serves as the base unit responsible for converting the received high frequency signals to more usable IF's and to prepare the signals for further processing stages.

Rx Antenna

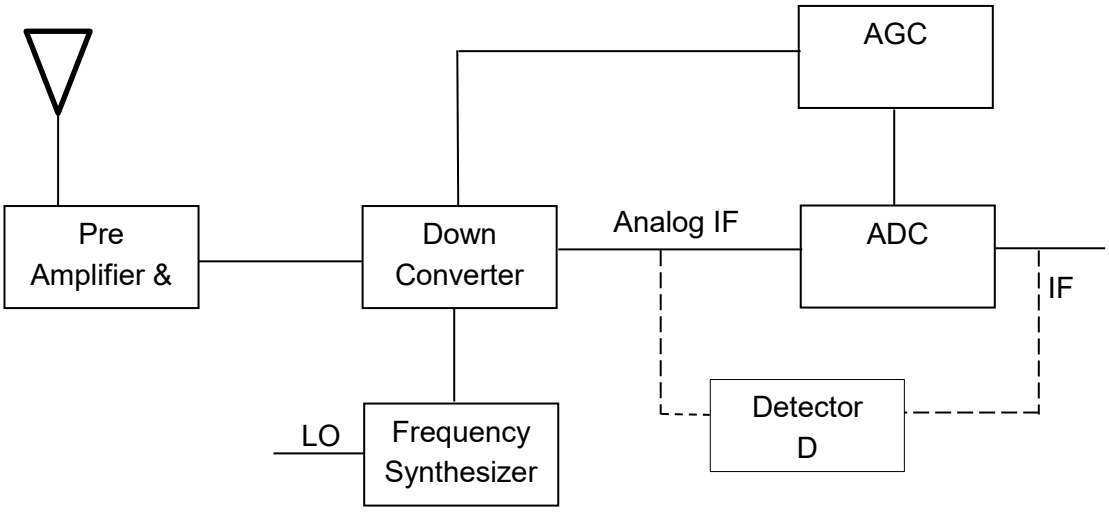

Figure 5. Simple block diagram of a GNSS receiver front end compatible with L1 frequency band [12].

A typical GNSS receiver front end compatible with L1 frequency band consists of an antenna, a pre-amplification & filtering stage, local oscillator (LO), downconverter and Analog to digital converter (ADC) [12].

Let's take a brief look at the functionality of each stage,

- Antenna: The device will be designed to capture radio waves travelling at 1575.42MHz (L1 frequency band). The performance of the antenna device is described by parameters such as voltage wave standing ratio, impedance, polarization, gain pattern among others.
- Filtering and pre-amplification: Due to poor frequency selective nature of a GNSS antenna, proper filtering is required to allow only required frequencies and eliminate other high frequency signal components. To accomplish this, a filter with band pass characteristics is used. Strength of the signals received by antennas are always weak, so it necessary to rise the magnitude of signals that falls within the required frequency range. This is done by an amplifier described by factors gain and noise figure.

- Down converter: Analysis of signals at high frequencies such as 1575.42MHz would need extremely complex components that are often expensive, thereby it is necessary to reduce such high frequencies to more usable frequencies know as intermediate frequency (IF) without compromising the characteristics of the original received signal. In this case, the received 1575.42MHz signal is down converted to an IF of 47.74MHz. This process is achieved by mixing the original signal with a 1527.68MHz signal generated by the LO and frequency synthesizer combination. The mixing process also results in unwanted higher frequency components (harmonics) which is removed by appropriate band pass filtering.
- ADC: The down converted filtered signal is then fed to the ADC operating at a sampling frequency of 38.192MHz. The output of ADC is a digital signal at an IF of 9.548MHz. To ensure the whole conversion process is carried out with minimal errors, ADC works in tandem with automatic gain control (AGC).

The down converted Analog signal of IF 47.7MHz is used as the base signal to assess the performance of the detection algorithm conceived in this study [12]. But the same detector can also be used to analyse the signal available at the output of ADC. Also, the values of IF at the output of Down converter and ADC varies for different receivers tuned to L1 band.

2.3 Wavelet Transforms

Before getting into the main topic, it is important to get a general idea of some basic concepts related to wavelet transforms.

2.3.1 Basic Concepts

Wavelets: Wavelets can be defined as fast decaying, short duration wavelike oscillations with a mean value of zero [3][9]. They are denoted by $\psi(t)$. An important characteristic feature of wavelet is, its ability to accurately analyse signals consisting of sharp variations that are well restricted in both time and frequency domain, something that cannot be achieved efficiently using Fourier transforms [9]. This is the primary advantage wavelet analysis has over Fourier analysis. Some of the application areas of wavelet analysis are denoising, compression (including image compression), analysis of signals and data in scientific research and so on.

Examples of wavelets are shown in figure 6 and figure 7. Oscillations or wavelets depicted here are also known as mother wavelets or base wavelets. Scaling them in time results in what is known as daughter wavelets or scales each with different frequency.

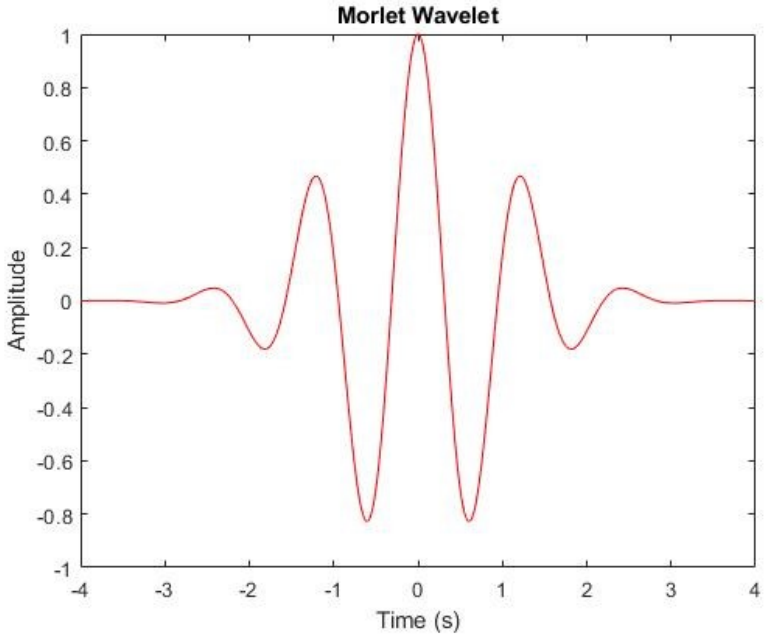

Figure 6. Analytic Morlet wavelet with [-4 4] effective support.

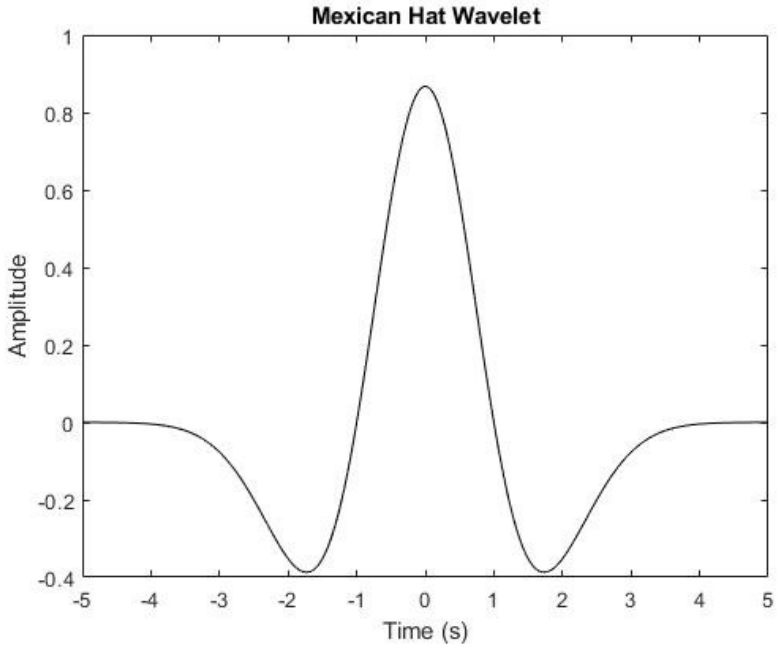

Figure 7. Mexican hat wavelet with [-5 5] effective support. It is the 2nd derivative of the gaussian probability density function.

Scaling: Scaling is a process of expanding or compressing a signal in time. Scaling can be mathematically expressed as [9],

$$\Psi(t/s) \tag{2.1}$$

where s is the scaling factor and $s > 0$.

Case 1: If $s > 1$, then

The process of scaling results in a stretched wavelet, which is depicted in figures 8 and 9.

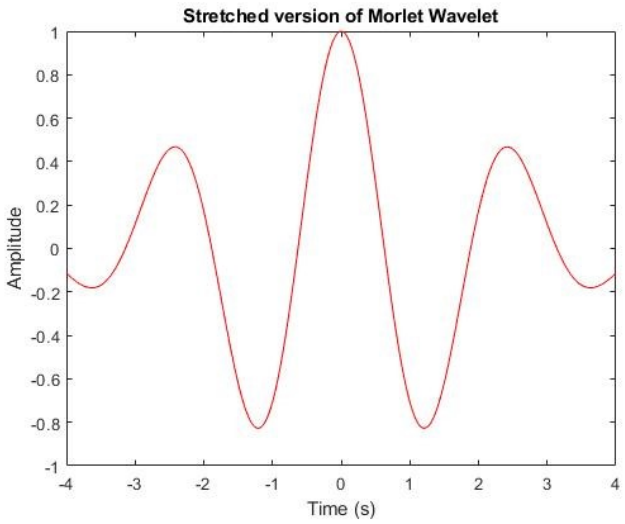

Figure 8. Stretched version of Morlet wavelet (scaling factor *s* = 2).

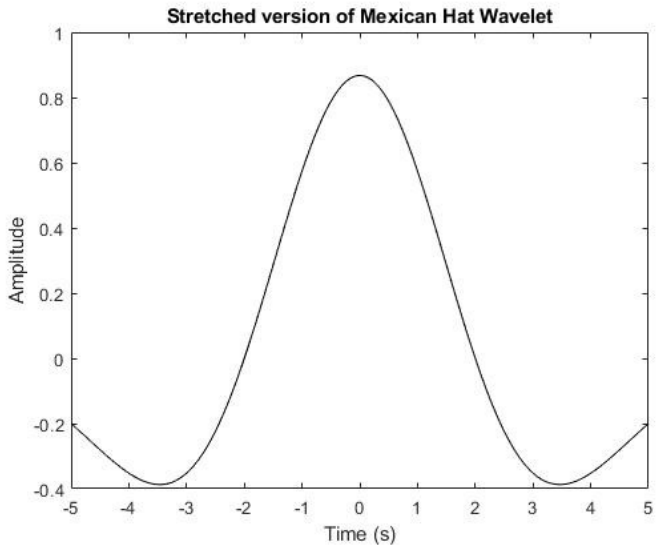

Figure 9. Stretched version of Mexican hat wavelet (scaling factor *s* = 2).

Case 2: If $0 < s < 1$, then

The process of scaling results in a compressed wavelet, which is depicted in figures 10 and 11.

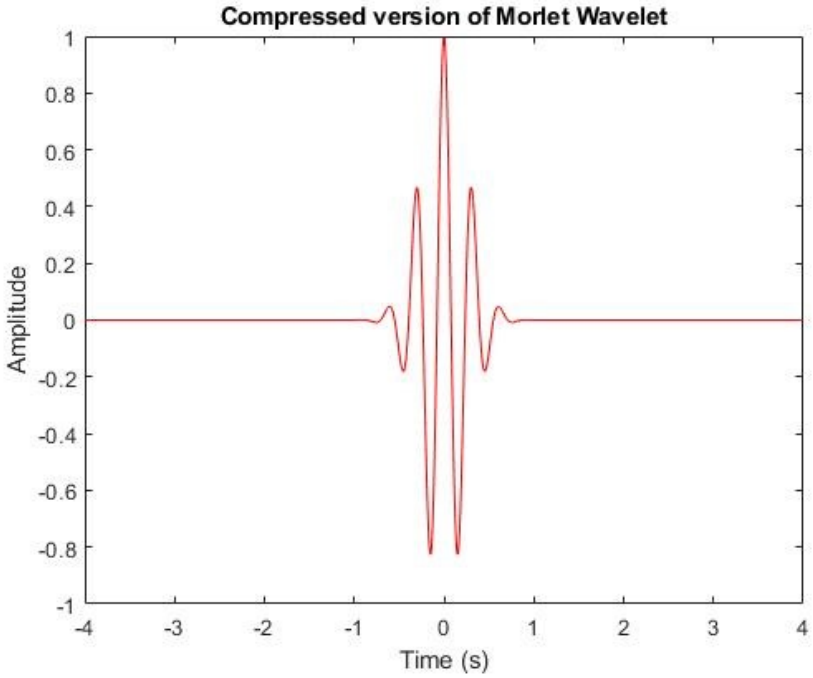

Figure 10. Compressed version of Morlet wavelet (scaling factor *s* = 0.25).

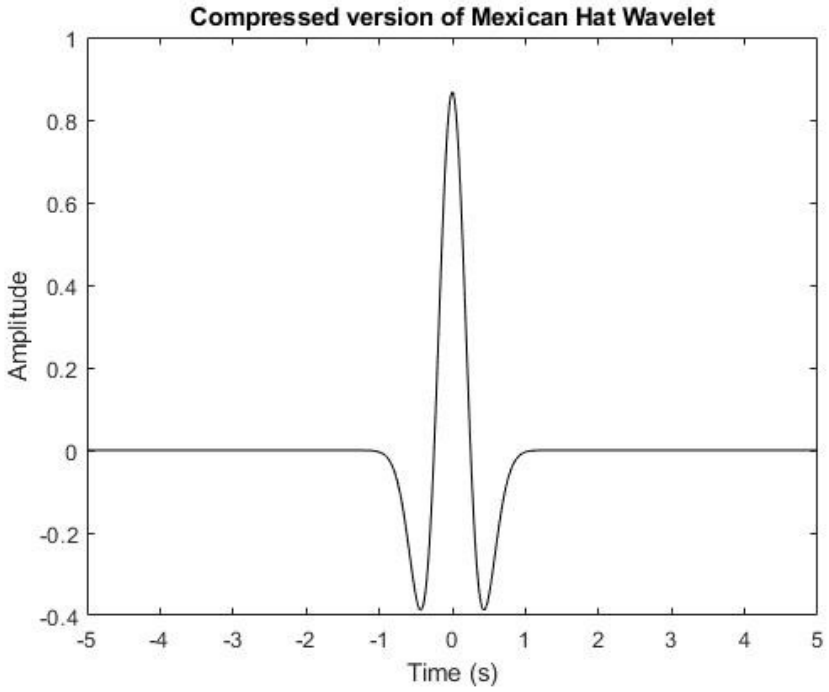

Figure 11. Compressed version of the Mexican hat wavelet (scaling factor *s* = 0.25).

Based on this, we can conclude that scaling factor s is inversely proportional to the frequency. Which means, case 1 results in lower frequency wavelets and case 2 results in higher frequency wavelets. The resulting equivalent frequency can be represented mathematically as,

$$F_e = \frac{F_C}{(s*dt)} \tag{2.2}$$

where F_C = centre frequency of the wavelet (Mother wavelet) and *dt* = sampling interval.

A stretched wavelet captures steady variations in a signal on the other hand a compressed wavelet captures sharp variations.

Shifting: Shifting is a process that involves moving the wavelet along the duration of the signal and aligning it with certain characteristics which helps in extracting valuable information [9]. Shifting can be mathematically represented as,

$$\Psi(t - a), \tag{2.3}$$

Where, a = shifting factor, which indicates centre of the wavelet.

Finally, the mathematical definition of a wavelet family is given by the equation,

$$\Psi_{s,a}(t) = \frac{1}{\sqrt{s}} * \psi(\frac{t-a}{s}) \tag{2.4}$$

Depending on the nature of scaling and shifting of wavelets, we can define two types of wavelet transforms,

1. Continuous Wavelet Transforms (CWT)
2. Discrete Wavelet Transforms (DWT)

2.3.2 Continuous Wavelet Transforms

CWT involves shifting of wavelet scales (daughter wavelets) in time along the duration of the signal to be analysed and comparing it with the same original signal [9]. This process results in constants known as wavelet coefficients that are function of frequency and time. These wavelet coefficients help to characterise and capture the oscillatory nature of signals. Analytic wavelet family such as Morlet & Morse wavelets are suitable for CWT analysis. The applications of CWT include time – frequency analysis and filtering of frequency components that are localised in time [8][9].

CWT can be represented mathematically as,

$$R_{\psi}(a,s) = \frac{1}{\sqrt{s}} * \int_{-\infty}^{\infty} r(t) * \psi(\frac{t-a}{s})\, dt \qquad (2.5)$$

Where,

r(t) = received signal.

s = scaling factor.

a = shifting factor.

Ψ(t) = Base wavelet.

$R_{\psi}(a,s)$ represents resulting wavelet coefficients as a function of frequency & time or in other words function of wavelet scaling parameter s and wavelet shifting parameter a.

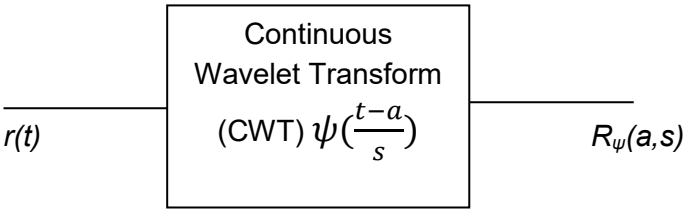

Figure 12. Simple block diagram of CWT algorithm with the input and output.

CWT can be interpreted as convolution of the input signal *r(t)* with a set of wavelet scales $\psi(\frac{t-a}{s})$ computed from the mother wavelet $\psi(t)$. For example, if a signal *r(t)* consisting of 10,000 samples is analysed with 50 wavelet scales, the CWT process results in 10,000 * 50 = 500,000 wavelet coefficients. In this way, CWT accurately captures and characterises the nature of a signal. Depending on the type of application, not all wavelet coefficients may be deemed useful. In that case, it is necessary to choose only those coefficients that contains valuable information, which can be achieved by careful selection of wavelet scales.

An interesting feature of CWT is its resistance to the noise present in a signal. Because of this property, Continuous Wavelet Transform is widely used in variety of scientific research areas such as, analysis of Electrocardiogram (ECG), study and analysis of natural phenomenon like earthquakes, Electroencephalography (EEG) and many more.

2.3.3 Discrete Wavelet Transforms

Discrete Wavelet Transforms (DWT) is a process comparing or filtering the received signal with a series of unique low pass and high pass filters resulting in approximation and detail coefficients respectively [9]. The process can be represented using block diagrams as shown below,

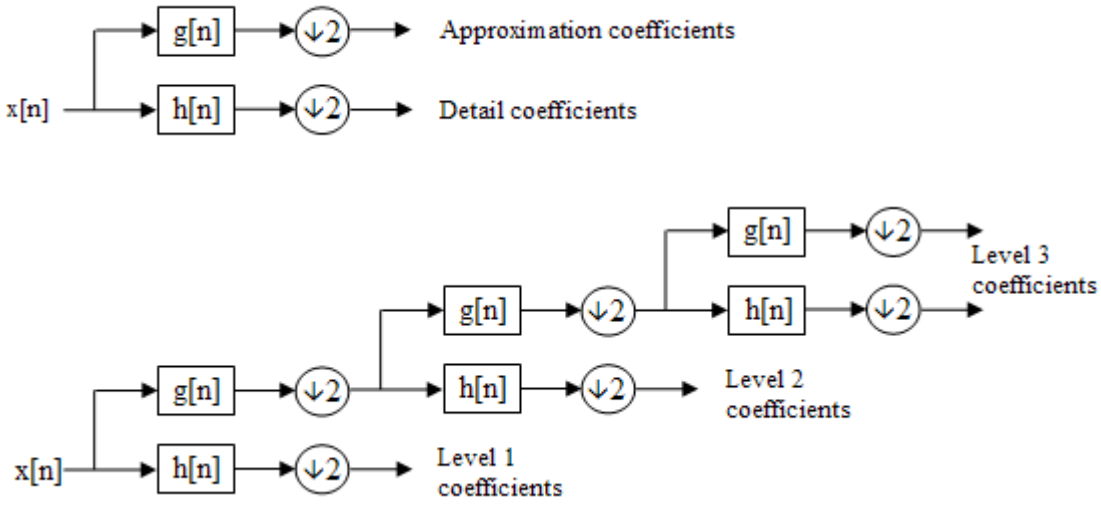

Figure 13. Block diagram depicting the process of DWT.

In DWT, the low pass and high pass filter functions g(n) and h(n) are unique to wavelets. The filters are also known as wavelet filters and scaling filters respectively. Depending on the nature of application, the input signal can be successively decomposed as shown in figure 13 to obtain better representation. After each decomposition level the filter outputs are down converted by a factor of 2 consistent with the Nyquist criteria [8][9]. DWT technique facilitates in analysing signals at increasingly narrower sub bands at distinct resolution, which is the essence of multi resolution analysis. DWT also helps in denoising and compression of signals [9]. The functions g(n) and h(n) can be related to the input x(n) mathematically as,

$$Y_L = (x * g)[n] \;\&\; Y_H = (x * g)[n] \tag{2.6}$$

Where,

Y_L = output of the low pass filter giving approximation coefficients.

Y_H = output of the high pass filter giving detail coefficients.

Both outputs will be subjected to down sampling after each level as shown in figure 13. Also, each filter level has different passbands with distinct centre frequencies.

As mentioned earlier in the text, DWT and CWT differ from each other on how scaling and shifting is accomplished. In the case of DWT, the mother wavelet $\psi(t)$ is scaled and shifted in powers of 2. Mathematically, such wavelet family can be represented as,

$$\Psi_{s,a}(t) = \frac{1}{\sqrt{v}} * \psi\left(\frac{t-kv}{v}\right) \quad (2.7)$$

Where,

$v = 2^i$

k = Shifting parameter of integer type (k = 1,2,3,4…).

i = Scaling parameter of integer type (i = 1,2,3,4…).

The base scale in DWT is set to 2, distinct scales can be obtained by raising the base scale to integer values as shown above and shifting is carried out at integer multiples defined by the term kv. This process is commonly known as dyadic scaling and shifting. The major advantage of dyadic scaling and shifting is the elimination of redundancy in coefficients, which makes DWT consume less memory compared to CWT [9]. DWT is also faster compared to CWT. DWT is also orthonormal.

In DWT, as depicted in figure 13 half of the samples are rejected after each filtering level consistent with Nyquist criteria. It may not be a good idea to reject samples as they may contain some information of interest. Also, conventional DWT assumes the size of the incoming signal is in powers of 2. If not, appropriate number of zeros will be padded to meet this requirement. To overcome this situation a variant of DWT known as ***Maximum Overlap Discrete Wavelet Transform (MODWT)*** is used [8].

MODWT differs from conventional DWT mainly in three ways,

- No down conversion (samples will not be rejected after each filtering level).
- It can be used to analyse signals of any size.
- Unlike DWT, MODWT retains redundancy.

Even with all these changes, MODWT retains all the characteristics of conventional DWT including multi resolution analysis. The detection algorithm presented in this study uses MODWT instead of DWT.

2.4 The Concept of Jamming

Intentional narrowband interference is a phenomenon where high powered signals are transmitted at certain frequencies to compromise the normal functionality of a system [1][6]. Intentional narrowband interference is commonly known as jamming. In this study, we are interested in high powered signals transmitted at GNSS L1 frequency band (1575.42MHz). Depending on the oscillatory nature, jamming signals are classified as,

- Class I Continuous Wave (CW) jamming signal [1][6][30].
- Class II chirp jamming signal (Linear type & Exponential type) [1][6][30].
- Class III chirp jamming signal with multi sawtooth function [1][6][30].
- Class IV chirp jamming signal with frequency bursts [1][6][30].

Class I CW jamming signals are signals transmitted at 1575.42MHz. It is a signal with constant amplitude and frequency which can be represented mathematically as,

$$J(t) = sin(\omega t) \tag{2.8}$$

where ω = 2πf & f = frequency (In this case, f = 1575.42MHz)

Class II chirp jamming signal is a signal where frequency rises or falls with time. Depending on the nature of rise or fall, ordinary chirp signals can be classified into two types,

- Linear chirp signal.
- Exponential chirp signal.

Mathematically they can be represented respectively as,

$$J(t) = sin(2\pi \left(f_0 * t + \left(\frac{r}{2}\right) * t^2\right)) \tag{2.9}$$

Where, $r = \frac{f_1 - f_0}{T}$ = rate of change of frequency.

f_0 = initial frequency & f_1 = final frequency.

T = time the signal takes to transit from f_0 to f_1.

$$J(t) = sin(2\pi f_0 \left(\frac{r^t - 1}{\ln(t)}\right)) \tag{2.10}$$

Where, $r = (\frac{f_1}{f_0})^{\frac{1}{T}}$

T = time the signal takes to transit from f_0 to f_1.

The frequency of the signal either vary linearly or exponentially with time.

Class III jamming signals contain multiple saw tooth functions as opposed to one saw tooth function in class II chirp as explained above. Also, class III chirp signals have multiple distinct frequency ranges.

Class IV jamming signals consists of multiple frequency bursts or pulses often around the main lobe of the GNSS L1 signal spectrum. Also, they are strong enough to differentiate from the noise present in the signal.

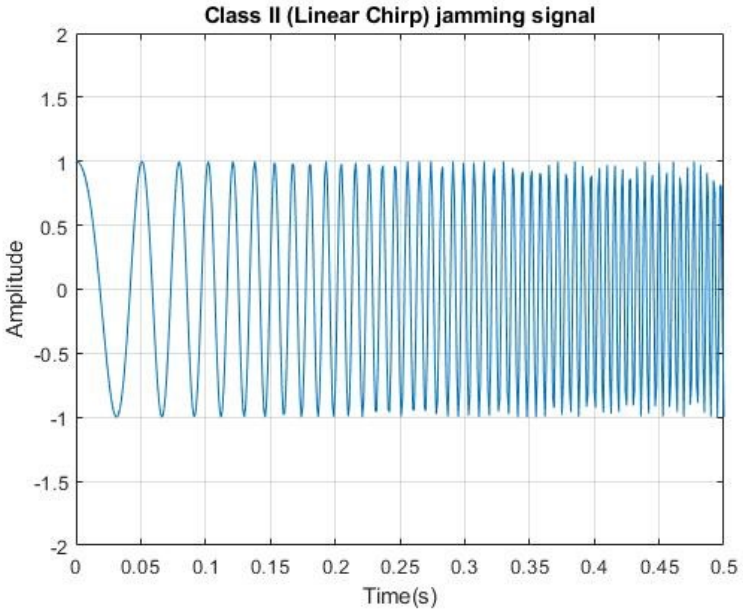

Figure 14. Class II linear chirp signal

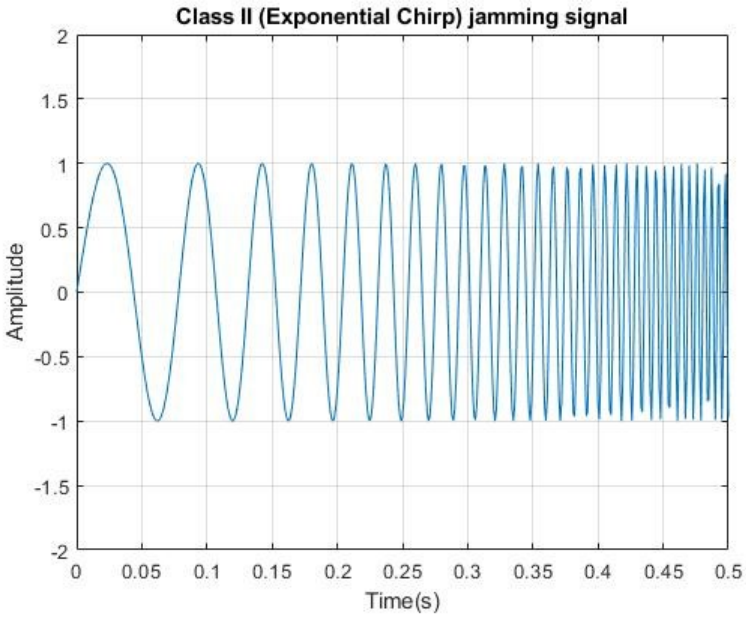

Figure 15. Class II exponential chirp signal

Figures 14 and 15 describe the frequency transition of linear chirp and exponential chirp respectively.

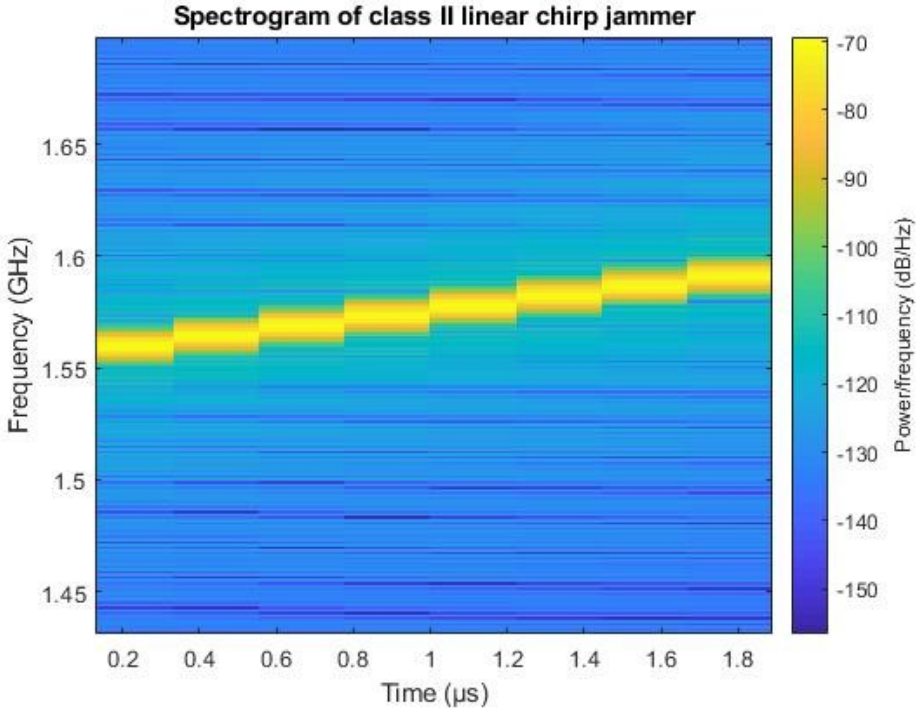

Figure 16. Spectrogram of class II linear chirp signal.

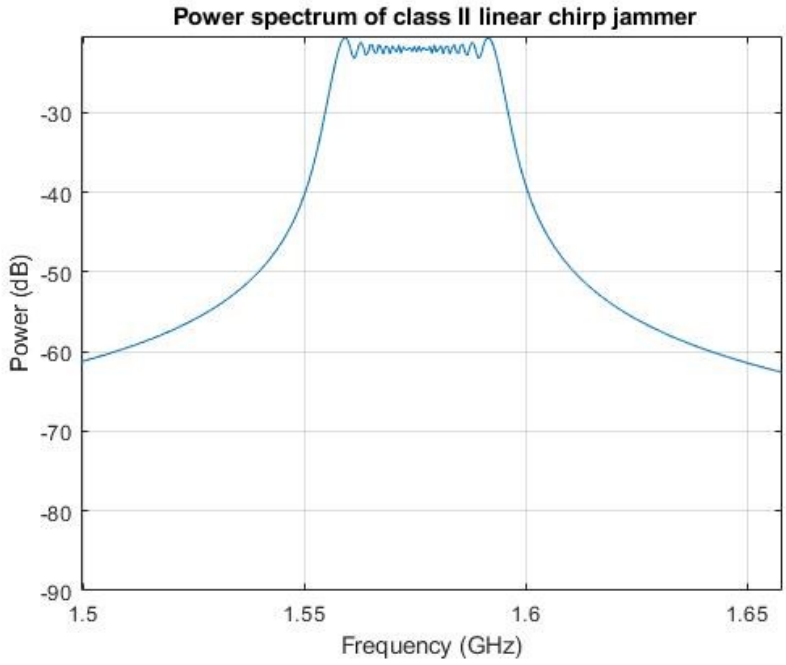

Figure 17. Power spectrum of class II linear chirp signal.

Figure 16 shows how frequency of a linear chirp varies with time and figure 17 describes the power concentration of linear chirp signal (approximately between 1.565GHz and 1.585GHz).

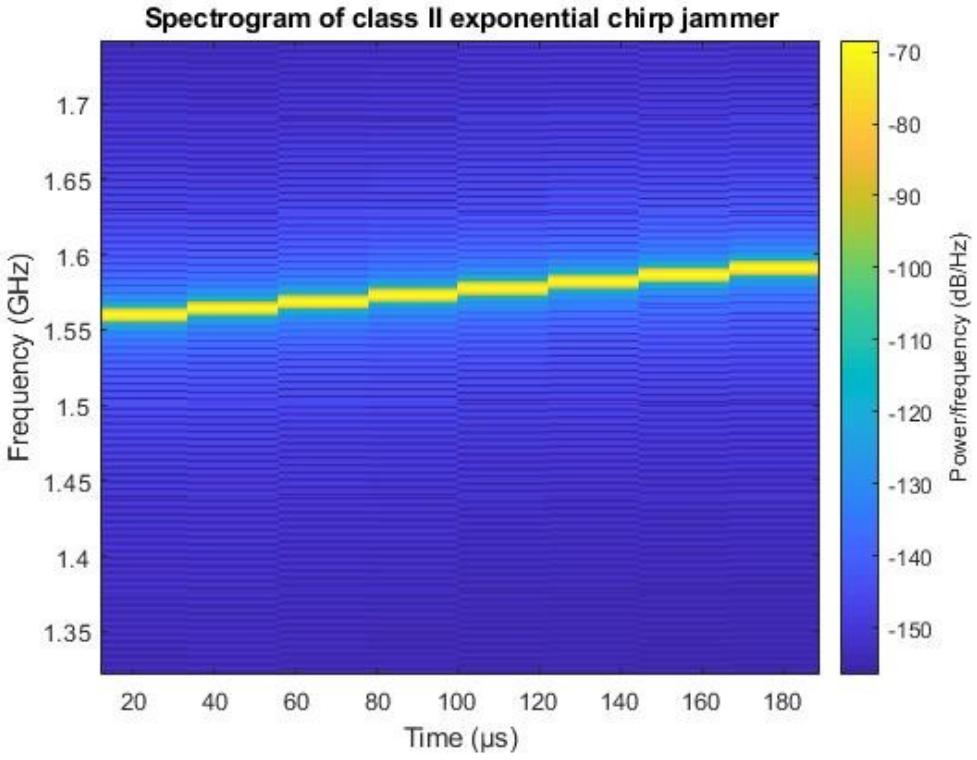

Figure 18. Spectrogram of class II exponential chirp signal.

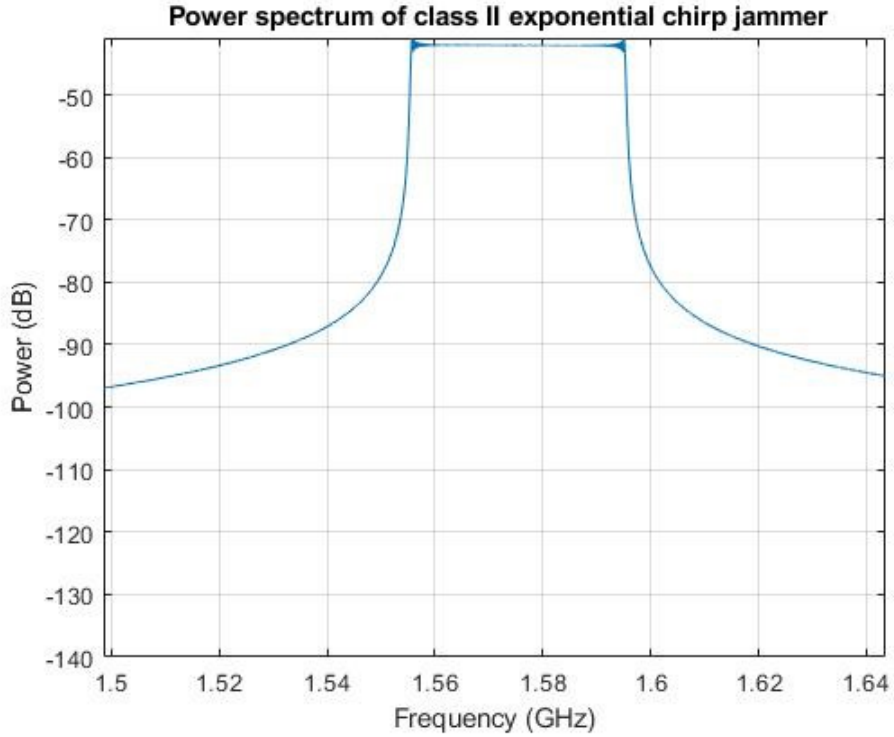

Figure 19. Power spectrum of class II exponential chirp signal.

Figure 18 shows the frequency variation of an exponential chirp with time and figure 19 describes the power concentration of exponential chirp signal (approximately between 1.55GHz and 1.59GHz).

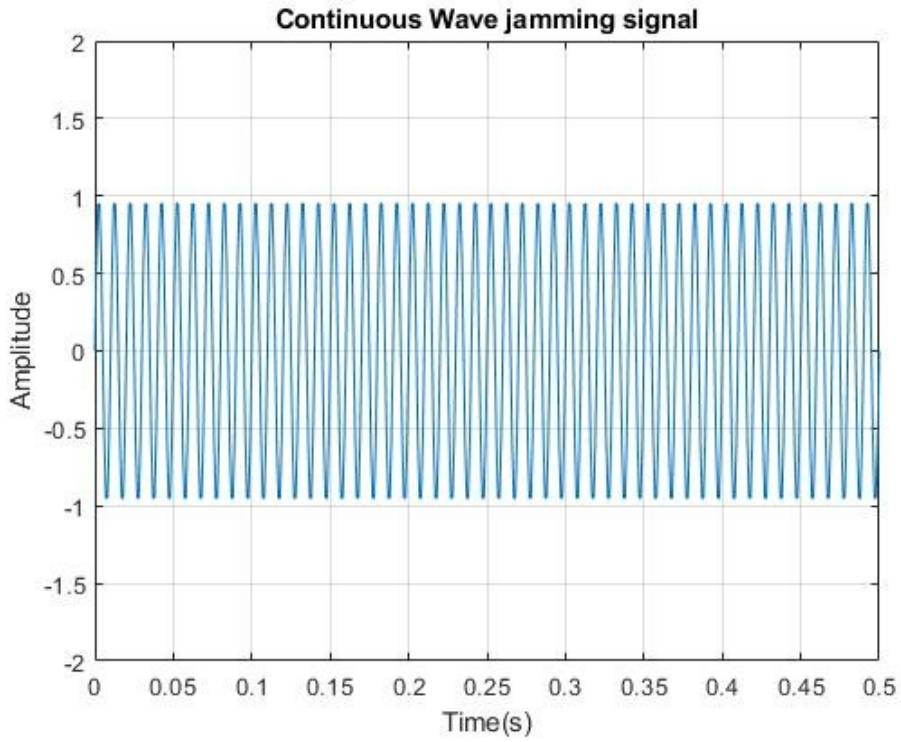

Figure 20. Class I CW signal

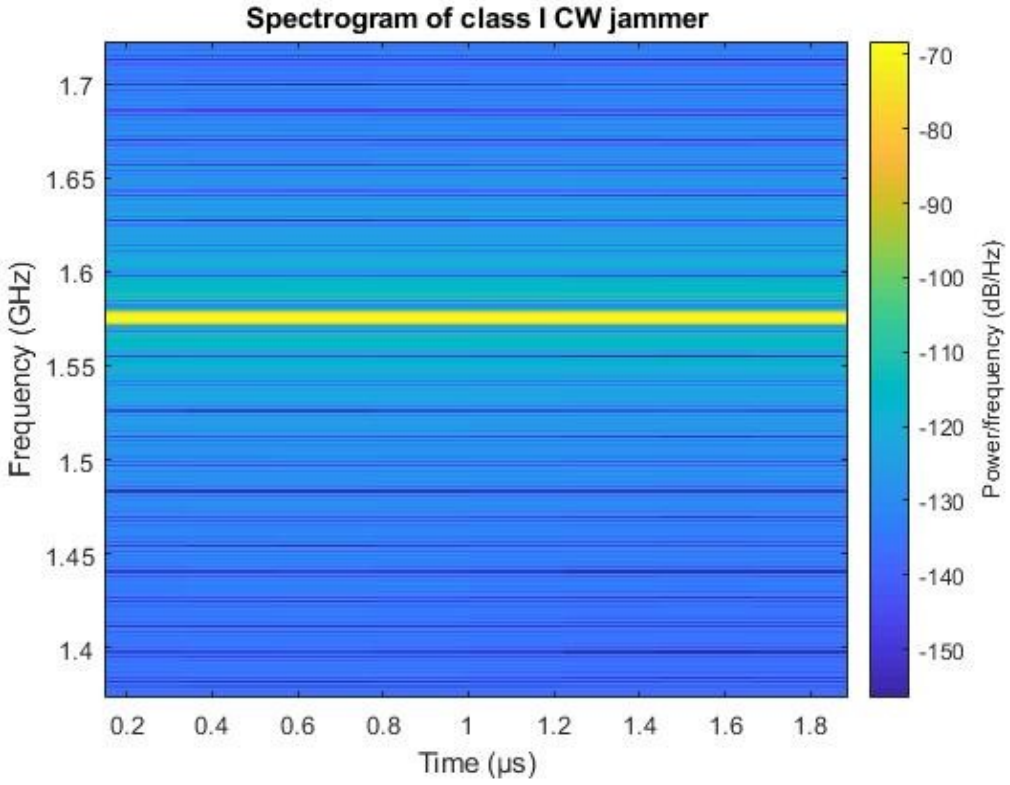

Figure 21. Spectrogram of class I CW signal.

Figure 20 depicts a CW jamming signal and figure 21 demonstrates the frequency variation of a CW jamming signal with time.

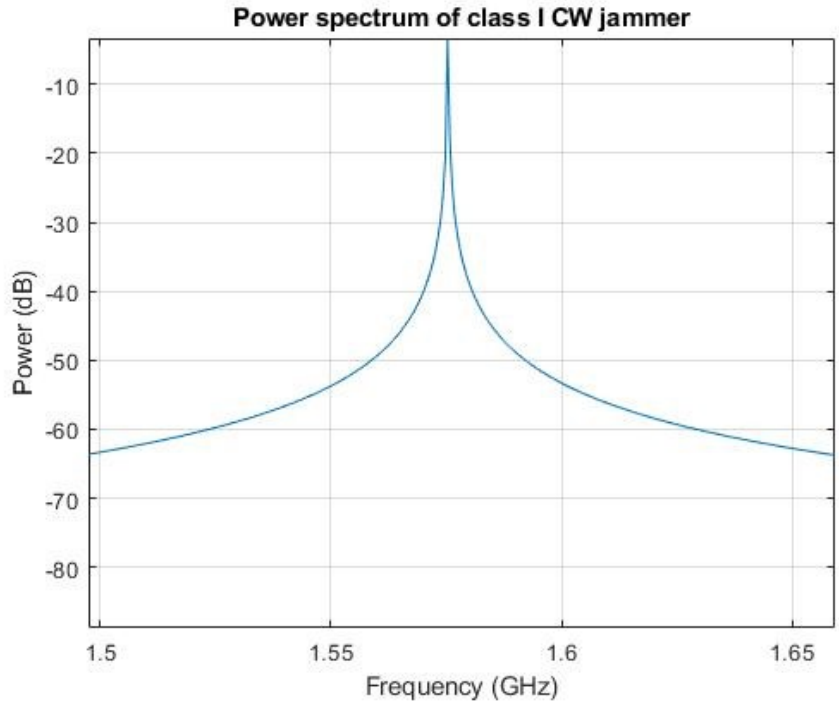

Figure 22. Power spectrum of class I CW signal.

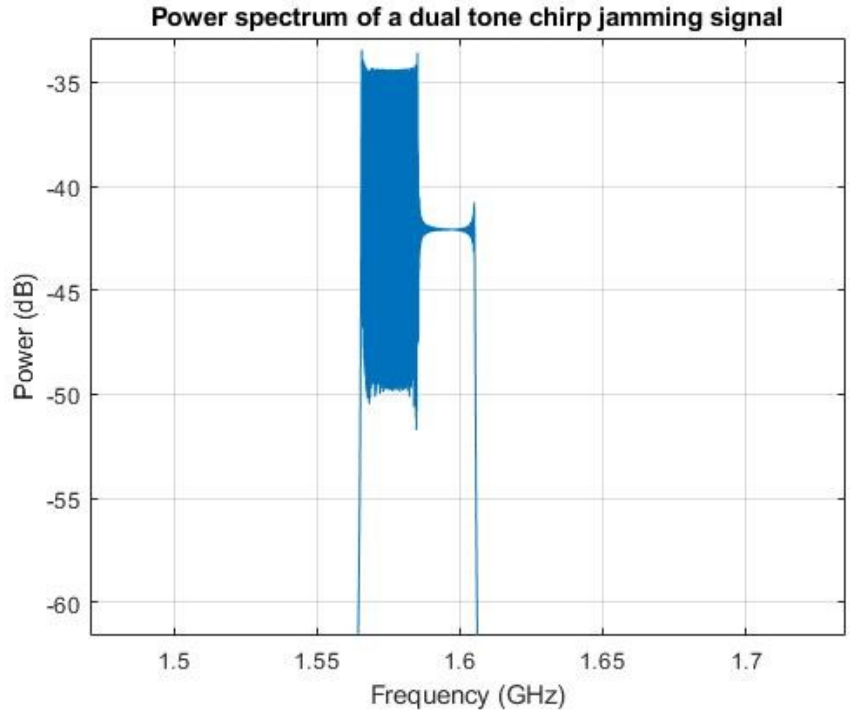

Figure 23. Power spectrum of a dual tone chirp jamming signal.

Figure 22 describes the power concentration of a CW jamming signal (at 1.575GHz) and figure 23 describes the power concentration of a dual tone chirp signal (between two frequency bands approximately from 1.56GHz to 1.61GHz and 1.56GHz to 1.58GHz, identified based on uneven power levels).

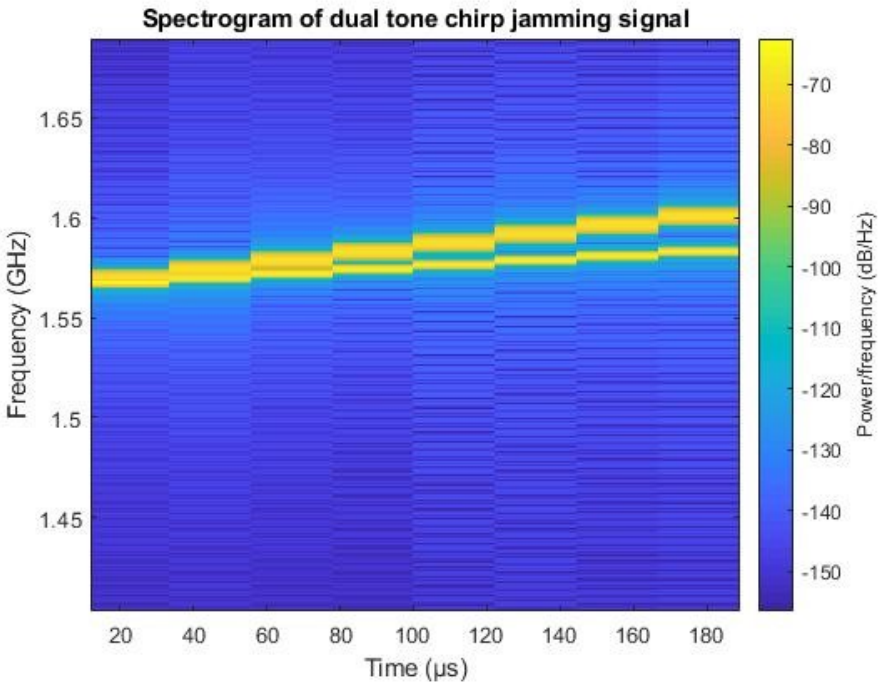

Figure 24. Corresponding spectrogram of the dual tone chirp jamming signal shown in figure 23 along with duration of frequency transition.

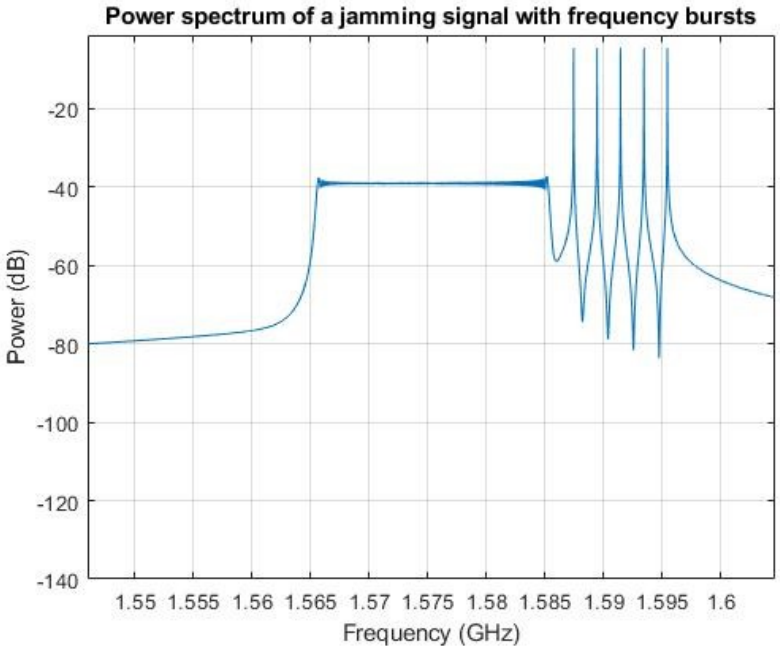

Figure 25. Power spectrum of a jamming signal with frequency bursts.

Figure 25 shows a chirp jamming signal with multiple frequency bursts between 1.58GHz and 1.6GHz.

Spectrogram is a time-frequency visual representation of a signal created using Fourier transform. If the same visual representation is created using wavelet transform, then it is known as *Scalogram*[13].

2.5 The Detection Algorithm

The detector developed in this study is designed to identify intentional interference components affecting the GNSS L1 transmission band. Its basic functionality is illustrated in the figure shown below,

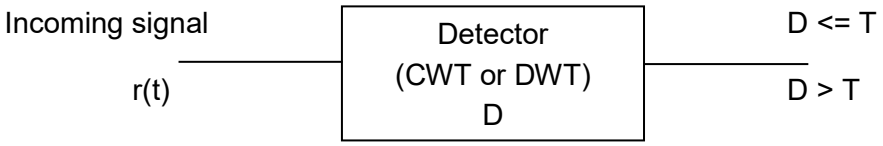

Figure 26. Simplified block diagram representation of the designed detector.

Assumptions and supporting framework:

- The source of interference (jamming) is unknown, means we have no knowledge of the interference parameters including spectral and statistical characteristics. In such cases, Interference can be modelled as random [5].
- At the front end of the GNSS receivers tuned to L1 band, the noise levels will be so high that the GNSS information signal will be completely buried in it. In this case, the received signal at this stage can be modelled as gaussian process [5].
- The software package used for simulation: MATLAB 2018b (licenced by Tampere University).
- The detection method used in this study is known as non-parametric Goodness of Fit (GoF) detection test [5][29].

Description of the detection process:

- ***Steps for CWT based detection algorithm:***
  1. CWT is obtained for the down converted reference signal at a suitable IF (in this case 47.7MHz) in the absence of jamming. The result would be a matrix of the form n x L with n indicating the number of wavelet scales and L indicating the length of the reference signal. It means that the reference signal is analysed with n number of wavelet scales each with a specific centre frequency. The value of n is chosen automatically by the CWT function.
  2. Since each wavelet scale represents a certain frequency, a wavelet scale close to the IF is selected.
  3. The power of this wavelet scale is estimated which will be used as reference value for comparison and is denoted as E.

4. Now, steps 1 to 3 is repeated for the actual down converted received signal at the same IF. The value estimated here will be the observed value and is denoted as O.
5. The reference value E is compared with the observed value O by taking the ratio $\frac{E}{O}$. This ratio is defined as the decision metric D.
6. D is compared with a suitable predefined threshold T. Choice of T depends on several factors and is extremely important.
7. A decision is made based on the logic,
    a. D <= T {jamming present}.
    b. D > T {jamming absent}.

- ***Steps for DWT based detection algorithm:***

1. MODWT is obtained for the down converted reference signal at a suitable IF (in this case 47.7MHz) in the absence of jamming. The result would be a matrix of the form 16 x L with L indicating the length of the reference signal and the number 16 indicates 15 different filtering levels with 15 (1 through 15) estimates of detail coefficients and one estimate of approximation coefficient at level 15.
2. Since each filtering level represents a filter passband with certain centre frequency, a detail coefficient estimated at a passband centre frequency close to the IF is selected.
3. One of the default output argument of MODWT is energy of the signal at different passbands with centre frequency. Estimated energy level of the reference signal at selected detail coefficient is recorded. This value will be used as reference value for comparison and is denoted as E.
4. Now, steps 1 to 3 is repeated for the actual down converted received signal at the same IF. The value estimated here will be the observed value and is denoted as O.
5. The reference value E is compared with the observed value O by taking the ratio $\frac{E}{O}$. This ratio is defined as the decision metric D.
6. D is compared with a suitable predefined threshold T.
7. A decision is made based on the logic,
    c. D <= T {jamming present}.
    d. D > T {jamming absent}.

In both CWT and MODWT, the centre frequencies at which the received signal is analysed is available as one of the output arguments of the wavelet transform function. This makes the selection process described in step 2 easy.

The efficiency of the detection algorithm is assessed by defining two parameters namely,

- *Detection probability (Pd)*: Jamming signal present (when a jamming signal is present). Pd can also be described as “True Positive”. Mathematically Pd can be represented as,

$$\text{Pd} = \frac{Number\ of\ times\ D \leq T\ (Expected\ outcomes)}{Total\ number\ of\ trials\ (All\ possible\ outcomes)}$$

- *False alarm probability (Pfa)*: Jamming signal present (when a jamming signal is not present). Pfa can also be described as “False Positive”. Mathematically Pfa can be represented as,

$$\text{Pfa} = \frac{Number\ of\ times\ D \leq T\ (Expected\ outcomes)}{Total\ number\ of\ trials\ (All\ possible\ outcomes)}$$

In this study, Pd is estimated for different values of JSR with SNR fixed. Pfa is a very important parameter which depends on the choice of threshold T. T in turn depends on how the decision metric D is defined. The value of T should be selected such that Pfa is as low as possible.

3. SIMULATION AND ANALYSIS

Before getting into the simulation and analysis part, it is necessary to provide proper explanation for certain assumptions made such as,

In the final section of the previous chapter, we have assumed that “if the noise strength (noise variance) at the front end of the receiver is very high compared to the strength of the GNSS received signal containing information, then the received signal can be modelled as gaussian process” [5]. This point needs to be justified.

For the sake of comparison, let’s call gaussian process as “Gaussian signal” and simulation of the received GNSS signal as “Actual signal”,

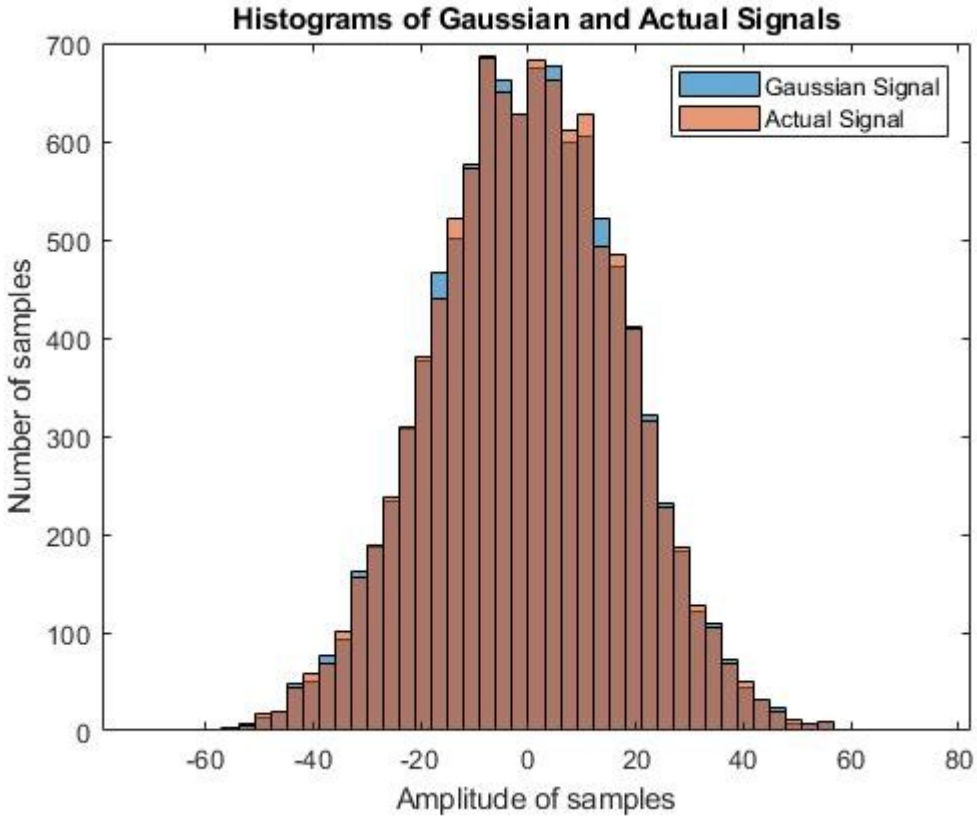

Figure 27. Histogram comparison between gaussian process and the simulation of the received GNSS signal.

From figure 27, it can be noted that the histograms of Gaussian process and simulation of the received GNSS signal overlap almost perfectly, which means the signals are nearly the same. Therefore, to simplify the entire detection process, the GNSS signal can be modelled as gaussian process.

3.1 Analysis of CWT based Detection Algorithm

MATLAB 2018b has an inbuilt, versatile CWT function that offers wide range of information about the signal of interest. The MATLAB command used to call the CWT function can be altered according to the requirement. The commands used in this study is of the form,

1. *[wt, F] = cwt (r, Fs);*
2. *cwt (r, Fs);*

The 1st command returns CWT of the received signal r along with centre frequencies (F) of the wavelet scales used in the process. Fs is the suitable sampling frequency applied as input. The 2nd command returns the magnitude scalogram plot. Magnitude scalogram is the representation of CWT coefficients as a function of time and frequency.

In this study, the family of wavelets used for analysis are analytic Morlet & Morse. Also, the selected CWT wavelet scale in the presence of jamming represents the analysis of actual received GNSS signal with jamming components and the scale in the absence of jamming represents the analysis of reference signal at the same point.

Simulation 1:

Jamming signal type: *Class 1 CW at 47.7MHz*, Wavelet family: *Morlet & Morse* & Ref. SNR = -25dB

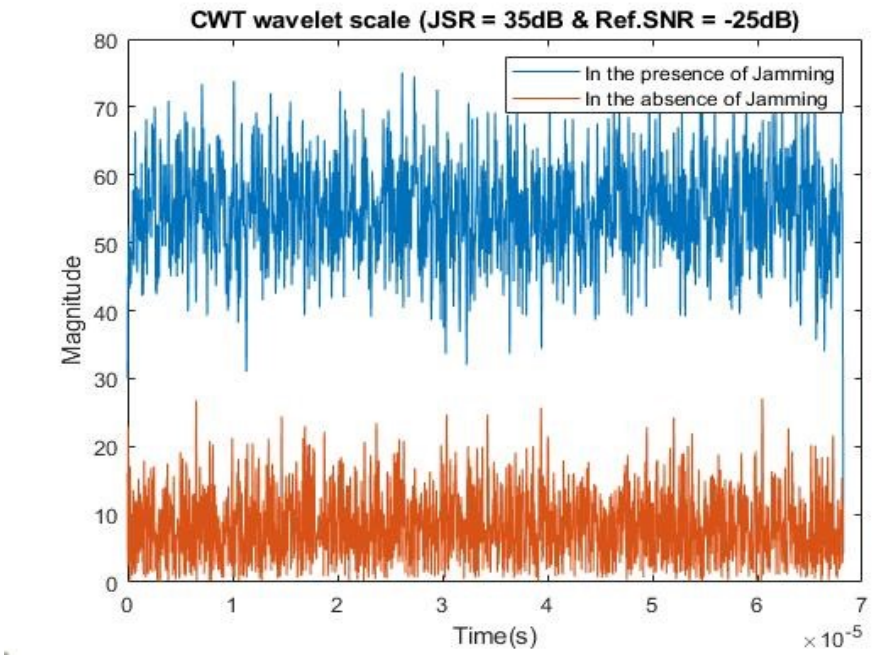

Figure 28. Comparison of selected wavelet scale in the presence of class I CW jammer and in the absence of jamming for JSR = 35dB.

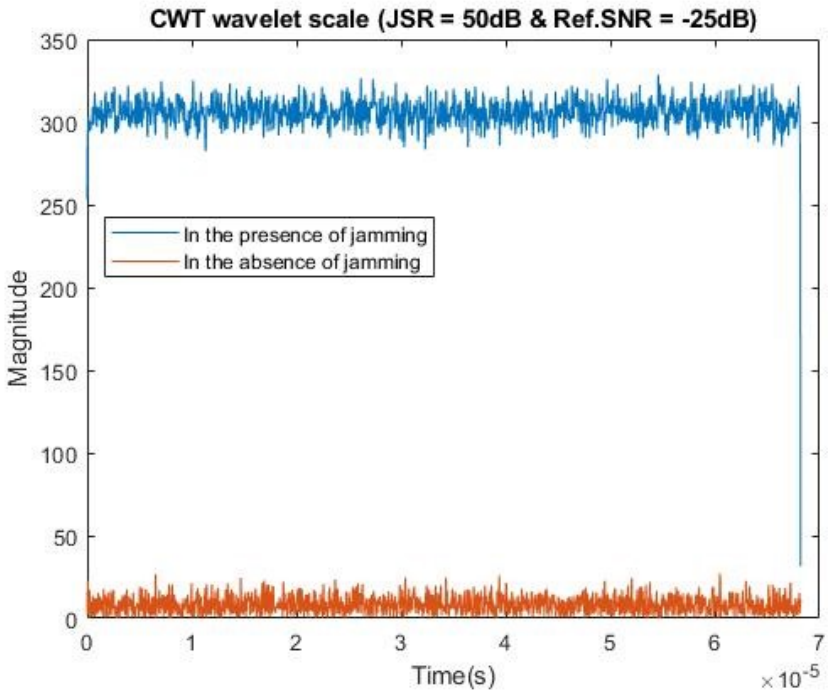

Figure 29. Comparison of selected wavelet scale in the presence of class I CW jammer and in the absence of jamming for JSR = 50dB.

Inference from figures 28 & 29: Higher the value of JSR, higher is the strength of the jamming signal compared to noise variance which makes the detection process efficient.

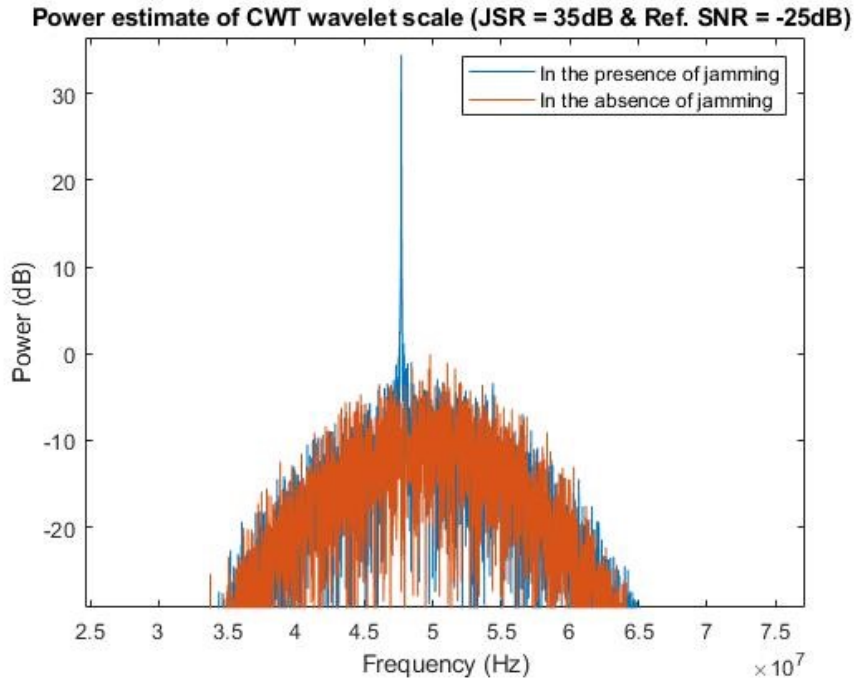

Figure 30. Power estimate comparison of the selected wavelet scale in the presence of class I jammer and in the absence of jamming for JSR = 35dB.

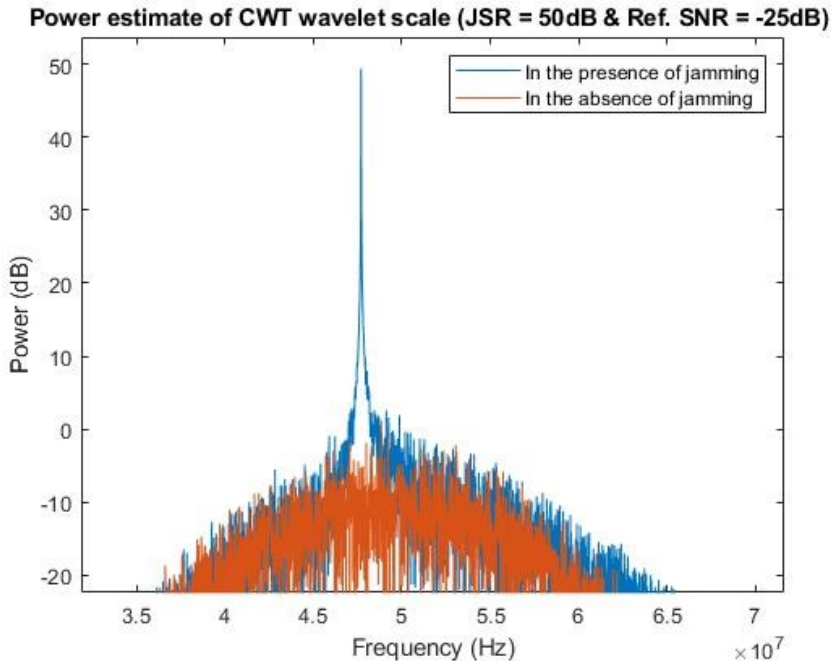

Figure 31. Power estimate comparison of the selected wavelet scale in the presence of class I jammer and in the absence of jamming for JSR = 50dB.

Inference from figures 30 & 31: Higher the value of JSR, higher is the power of the jamming signal which makes distinction and detection of jamming efficient (spike at 47.7MHz can be seen).

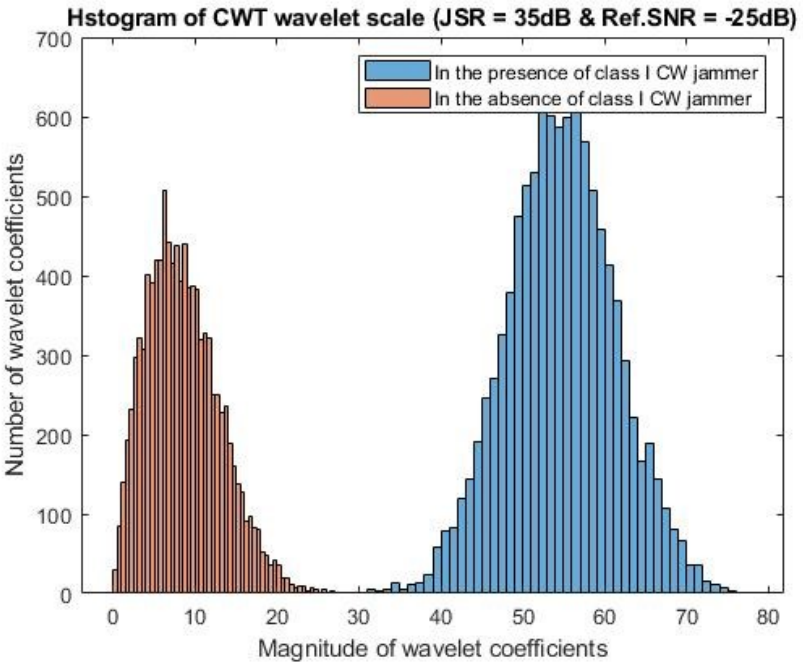

Figure 32. Histogram comparison of the selected wavelet scale in the presence of class I jammer and in the absence of jamming for JSR = 35dB.

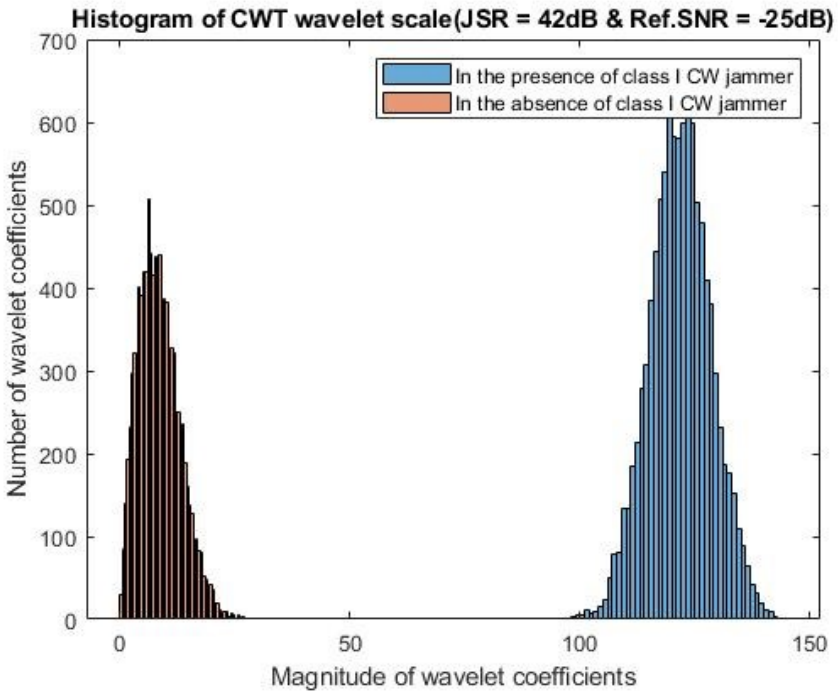

Figure 33. Histogram comparison of the selected wavelet scale in the presence of class I jammer and in the absence of jamming for JSR = 42dB.

Inference from figures 32 & 33: Higher the value of JSR, better is the distinction between two histograms which makes the detector efficient.

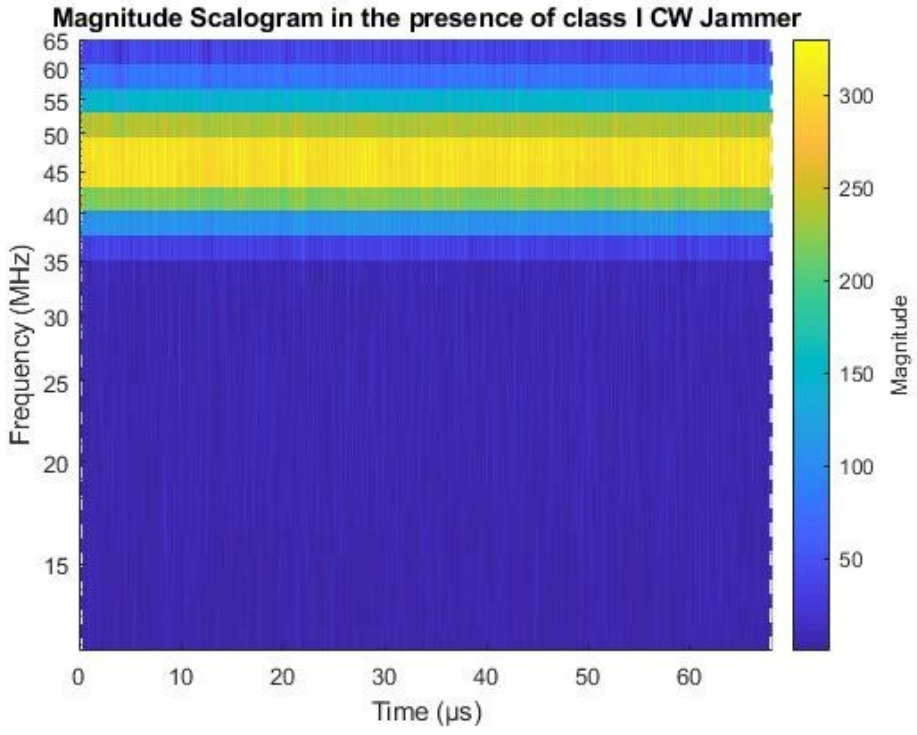

Figure 34. Magnitude scalogram in the presence of class I CW jammer at 47.7MHz.

Simulation 2:

Jamming signal type: *Class 2 single tone Chirp with 10MHz (from 42.7MHz to 52.7MHz centred at 47.7MHz) bandwidth,* Wavelet family: *Morlet & Morse* & Ref. SNR = -25dB

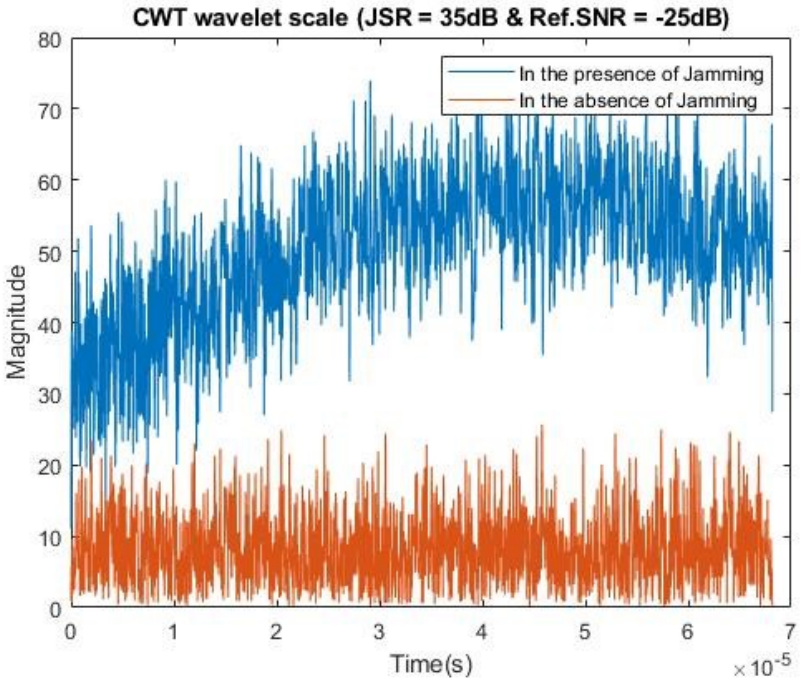

Figure 35. Comparison of selected wavelet scale in the presence chirp jammer and in the absence of jamming for JSR = 35dB.

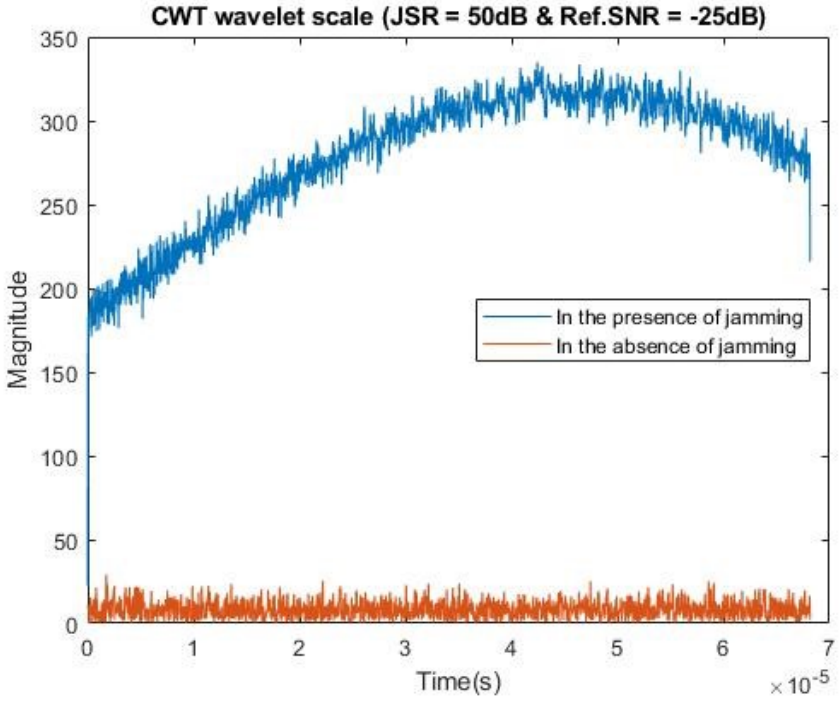

Figure 36. Comparison of selected wavelet scale in the presence of chirp jammer and in the absence of jamming for JSR = 50dB.

Inference from figures 35 & 36: Higher the value of JSR, higher is the strength of jamming compared to noise variance which makes the detection easy and efficient. The bend seen in the blue curve indicates the presence of a signal with certain bandwidth.

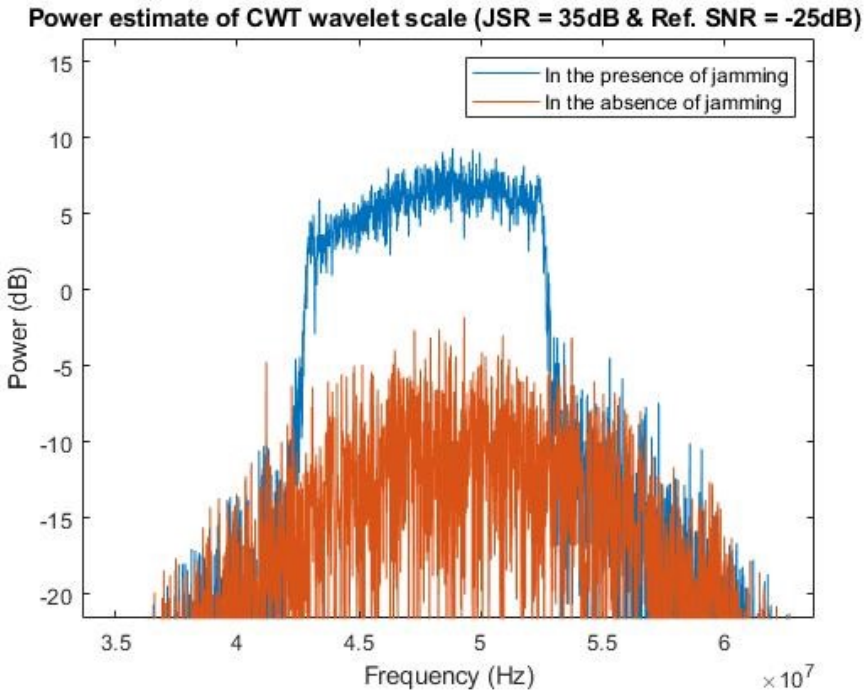

Figure 37. Power estimate comparison of the selected wavelet scale in the presence of chirp jammer and in the absence of jamming for JSR = 35dB.

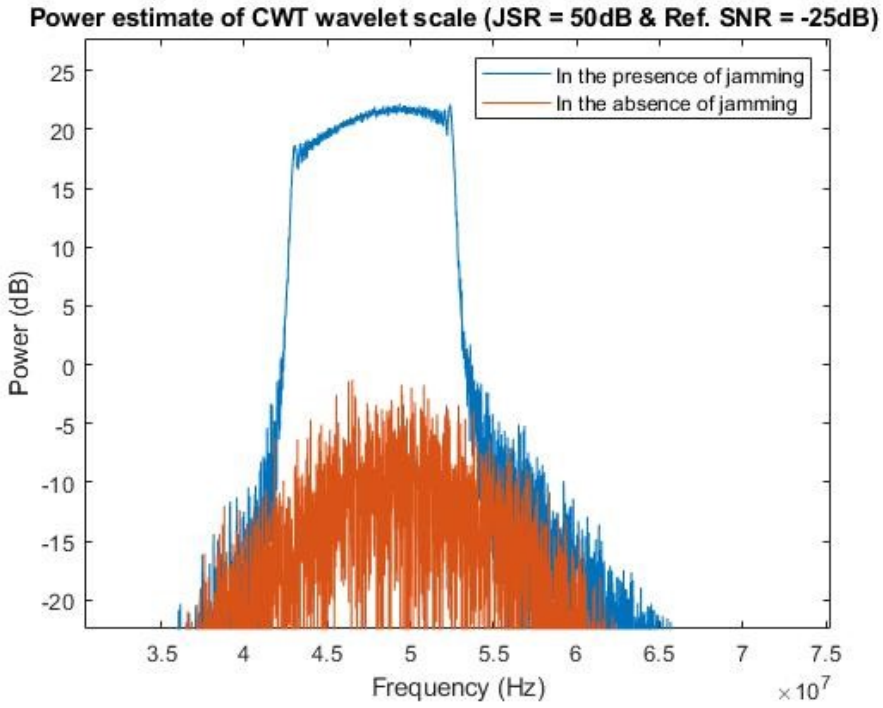

Figure 38. Power estimate comparison of the selected wavelet scale in the presence of chirp jammer and in the absence of jamming for JSR = 50dB.

Inference from figures 37 & 38: Higher the value of JSR, higher is the power of the jamming signal which results in clear distinction and efficient detection. High values of power can be seen from 42.7MHz to 52.7MHz, thereby indicating the presence of strong jamming signal.

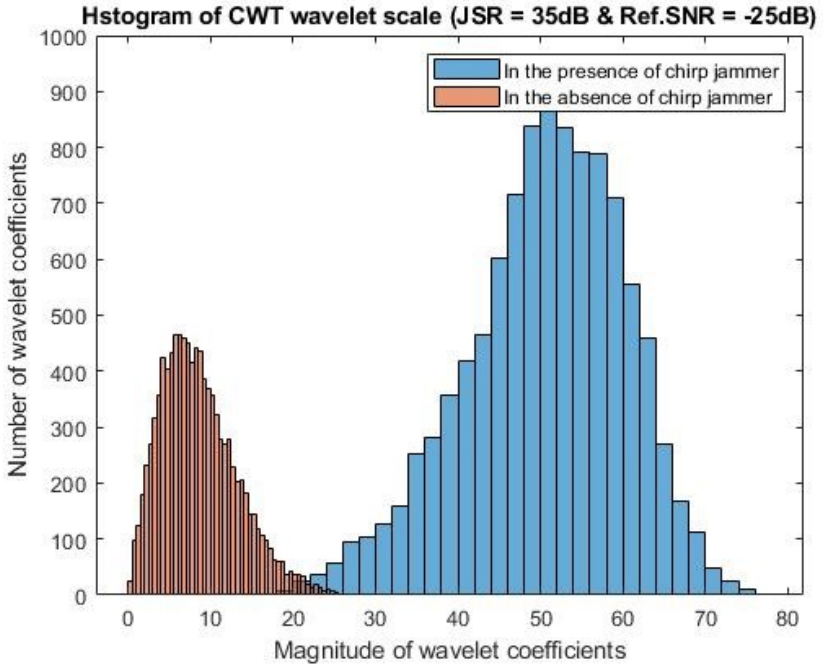

Figure 39. Histogram comparison of the selected wavelet scale in the presence of chirp jammer and in the absence of jamming for JSR = 35dB.

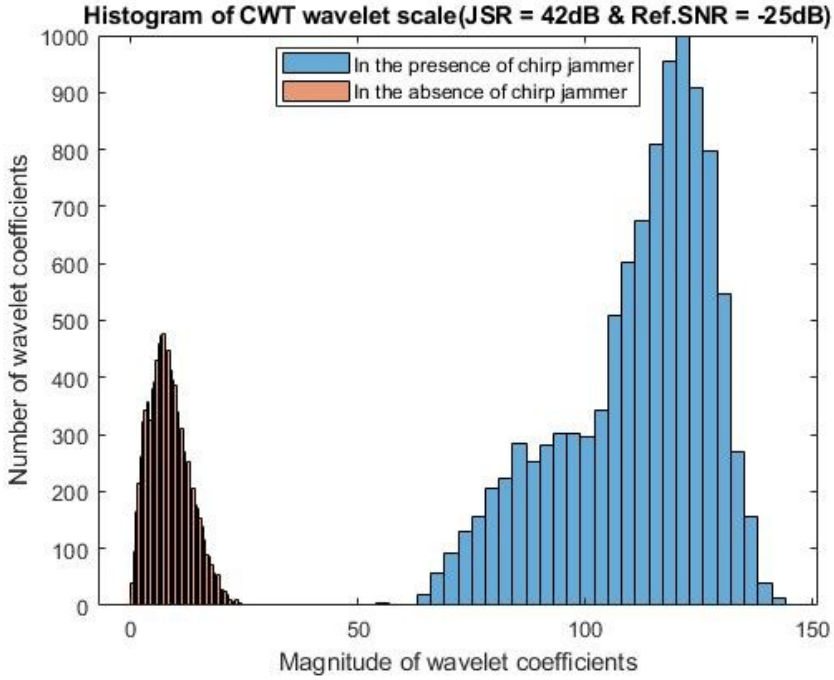

Figure 40. Histogram comparison of the selected wavelet scale in the presence of chirp jammer and in the absence of jamming for JSR = 42dB.

Inference from figures 39 & 40: Higher the value of JSR, better is the distinction between two histograms, thereby making the detector productive.

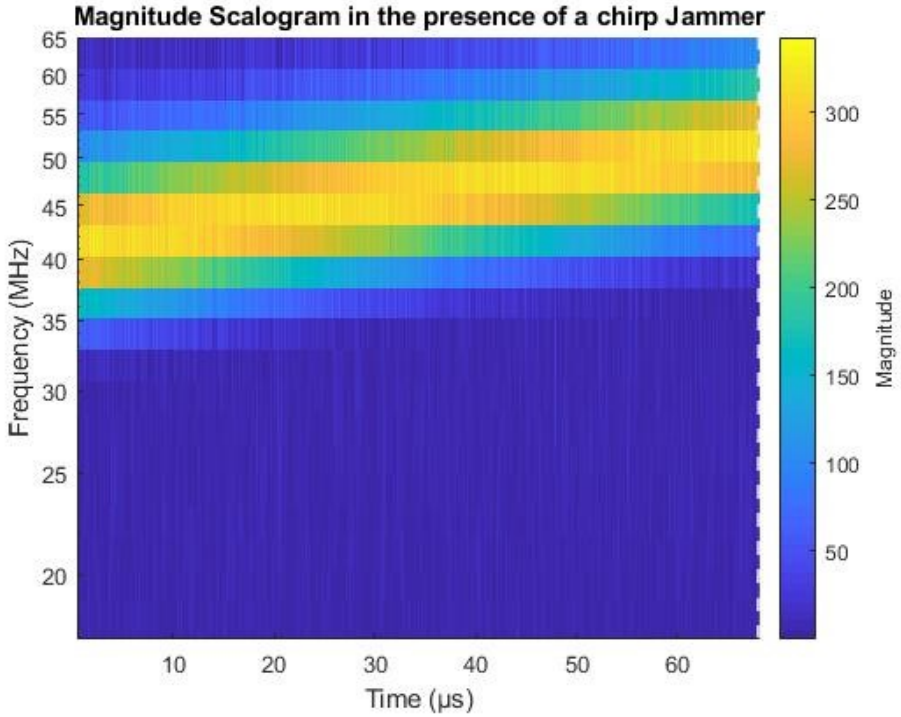

Figure 41. Magnitude scalogram in the presence of chirp jammer with bandwidth 10MHz. The bright yellow curve from approximately 42.7MHz to 52.7MHz.

Simulation 3:

In the absence of jamming, Ref. SNR = -25dB, Wavelet family: *Morlet & Morse*.

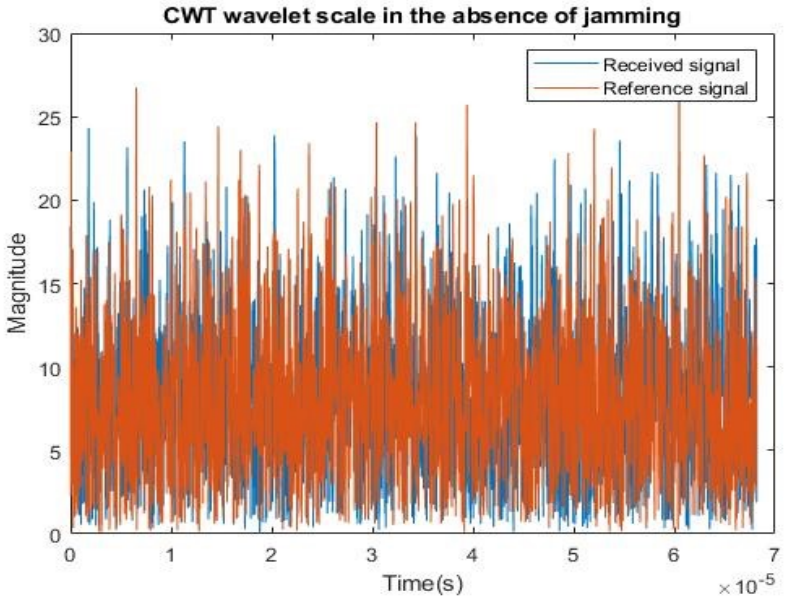

Figure 42. Comparison of selected wavelet scale of the received signal and the reference signal in the absence of jamming.

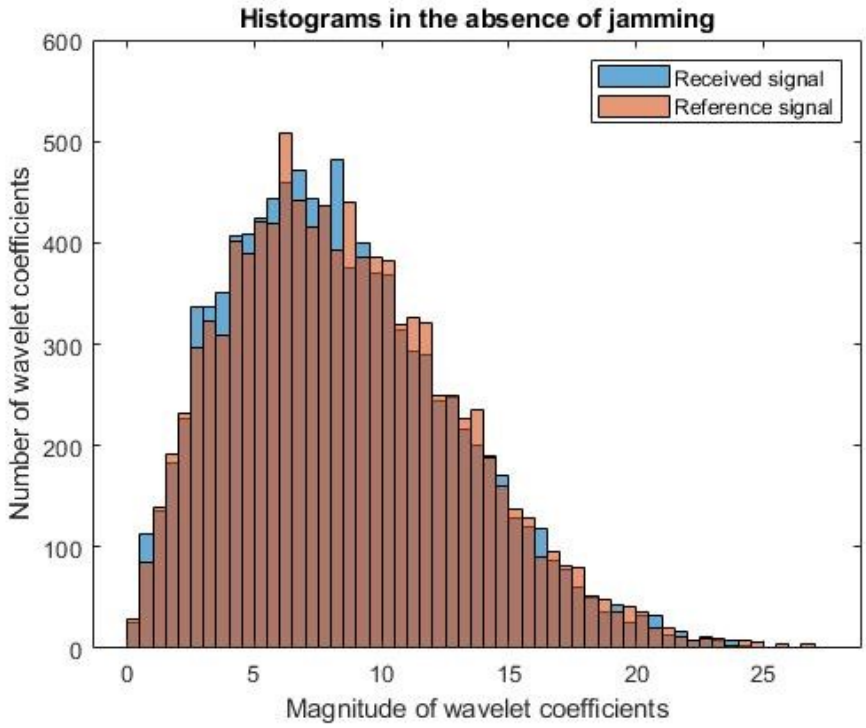

Figure 43. Histogram comparison of the received signal and the reference signal in the absence of jamming.

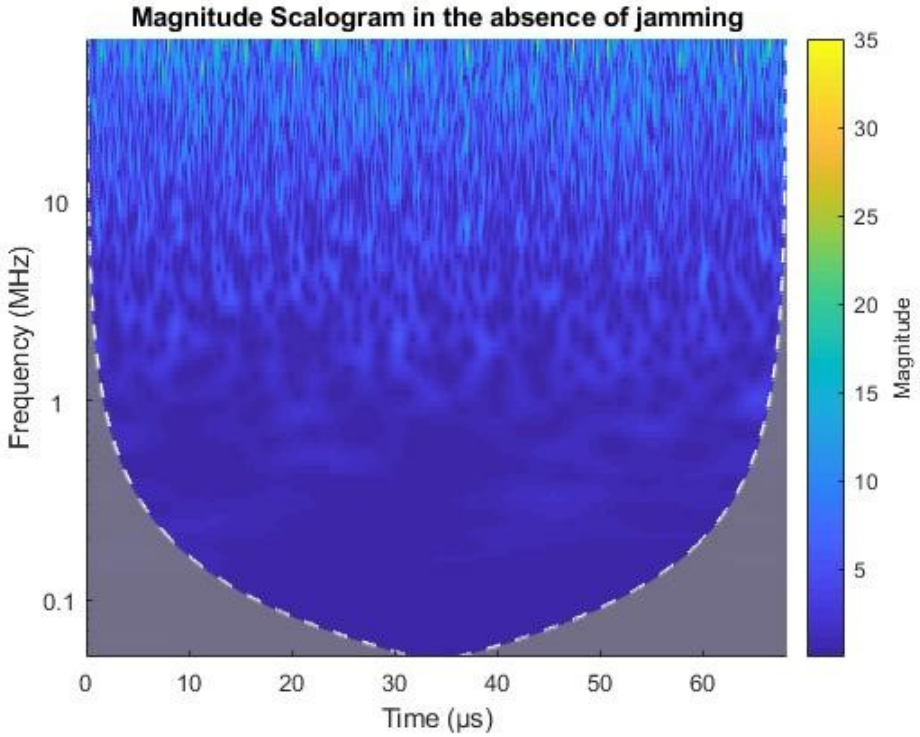

Figure 44. Magnitude scalogram in the absence of jamming.

Inference from figures 42 & 43: In the absence of jamming, the received signal and the reference signal are very similar (seen as overlaps in figures 42 and 43).

Simulation 4:

Jamming signal type: *Class 2 dual tone chirp with 10MHz (from 42.7MHz to 52.7MHz centred at 47.7MHz) and 6MHz (from 54.7MHz to 60.7MHz centred at 57.7MHz) band-width & a jamming signal with multiple frequency bursts at and around 47.7MHz,* Ref. SNR = *-25dB,* Wavelet family: *Morlet & Morse*.

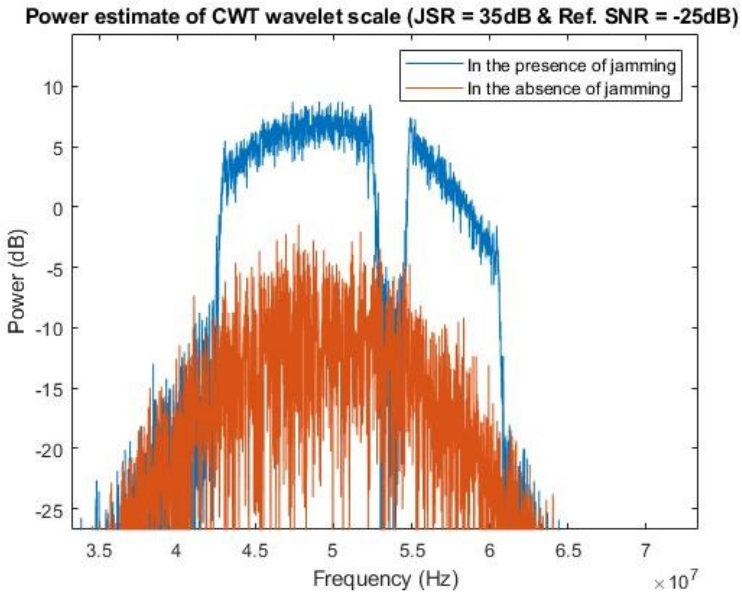

Figure 45. Power estimate comparison of the selected wavelet scale in the presence of dual tone chirp jammer and in the absence of jamming for JSR = 35dB.

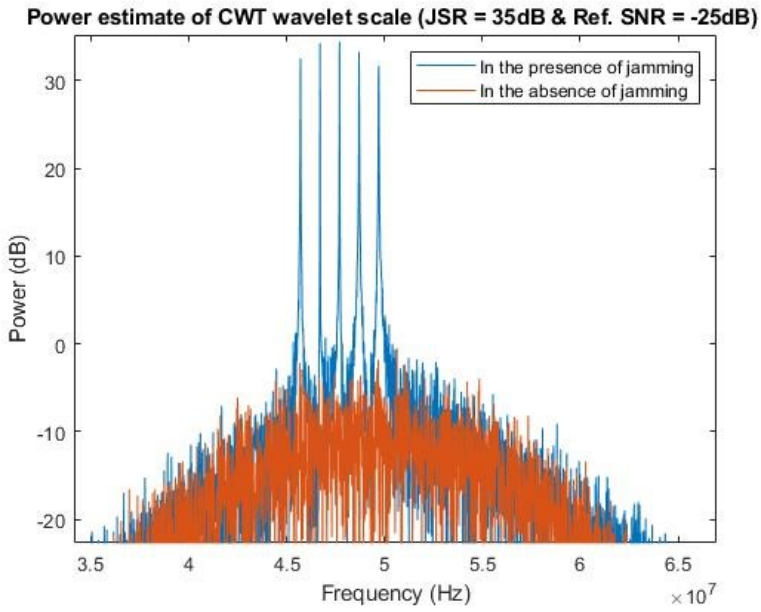

Figure 46. Power estimate comparison of the selected wavelet scale in the presence of jamming signal with multiple frequency bursts and in the absence of jamming for JSR = 35dB

3.2 Analysis of DWT based Detection Algorithm

MATLAB 2018b also has an inbuilt, versatile MODWT function that offers wide range of information about the signal of interest. Like CWT, the MATLAB command used to call the MODWT function can be altered according to the requirement. The command used in this study is of the form,

1. *[wt, ~, F, energy] = modwpt (r, 'wavelet name', 'TimeAlign', true);*

The *modwpt* function returns the details coefficients obtained after each level of filtering along with the final filter level approximation coefficient. It also returns the centre frequencies (F) of each filter level and energy of the signal of interest (r) in the filter passband. After each filtering level, the signal of interest experiences certain amount of delay, to compensate for this, 'TimeAlign' & true name – value argument pair is supplied as input. Also, *modwpt* function supports wide variety of orthogonal wavelet families which can be supplied as input under '*wavelet name*'.

The orthogonal wavelet family used in this study is called the symlet wavelet family, specifically *sym8* wavelet with 8 vanishing moments. Also, like CWT, the selected DWT detail coefficient in the presence of jamming represents the analysis of actual received GNSS signal with jamming components and the coefficient in the absence of jamming represents the analysis of reference signal at the same point.

Simulation 5:

Jamming signal type: *Class 1 CW jammer (at 47.7MHz)*, Wavelet used: *Sym8* & Ref. SNR = *-25dB*

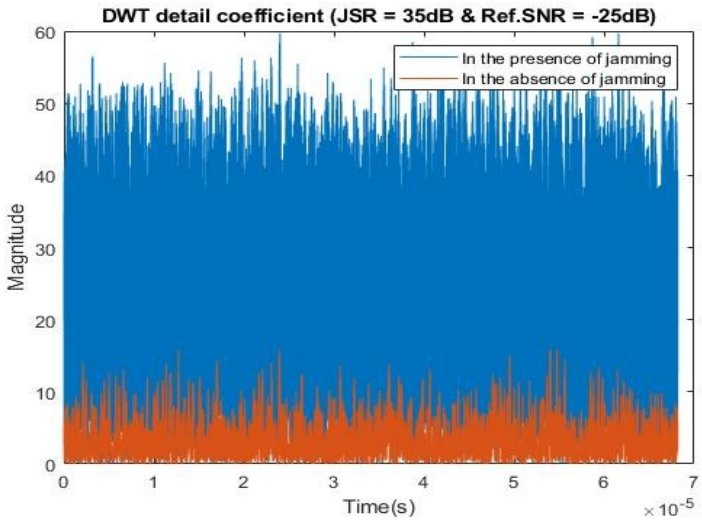

Figure 47. Comparison of selected detail coefficient in the presence of CW jammer and in the absence of jamming for JSR = 35dB.

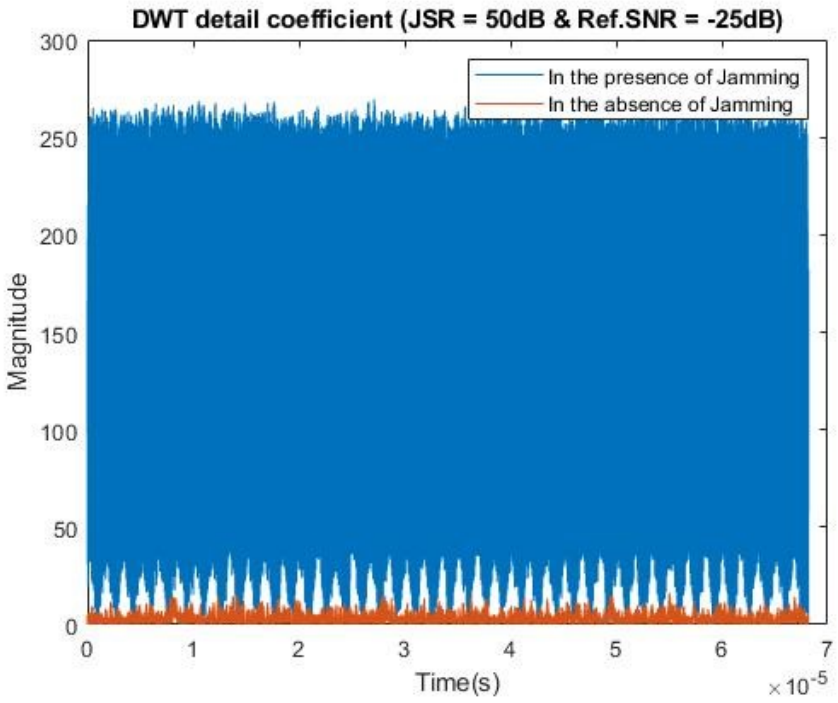

Figure 48. Comparison of selected detail coefficient in the presence of CW jammer and in the absence jamming for JSR = 50dB.

Inference from figures 47 & 48: Higher the value of JSR, easier it becomes to compare the received signal with reference signal resulting in better functionality of the detector.

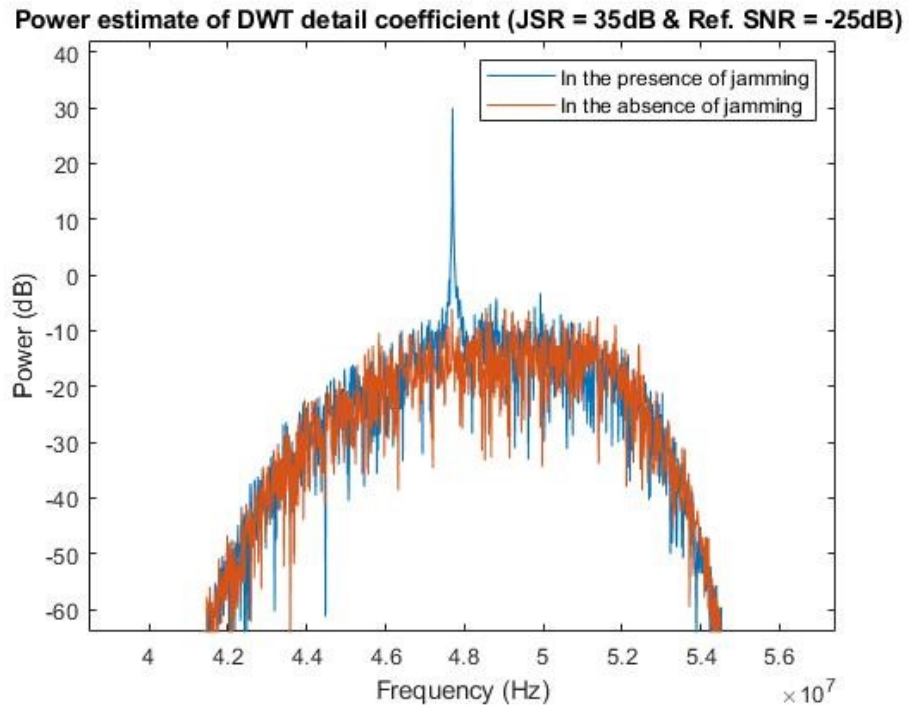

Figure 49. Power estimate comparison of the selected detail coefficient in the presence of CW jammer and in the absence of jamming for JSR = 35dB.

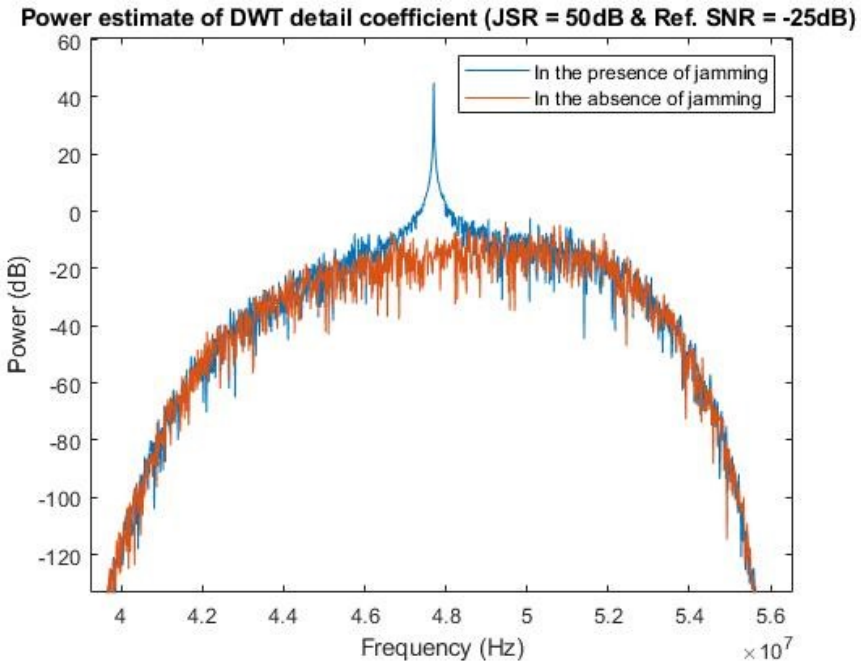

Figure 50. Power estimate comparison of the selected detail coefficient in the presence of CW jammer and in the absence of jamming for JSR = 50dB.

Inference from figures 49 & 50: Higher the value of JSR, higher is the strength of the jammer compared to noise variance, thereby improving the efficiency of the detector (Clear spike at 47.7MHz can be seen).

Simulation 6:

Jamming signal type: *Class 2 single tone chirp jammer with 10MHz (from 42 to 52.7MHz centred at 47.7MHz) bandwidth*, Wavelet used: *Sym8* & Ref. SNR = *-25dB*

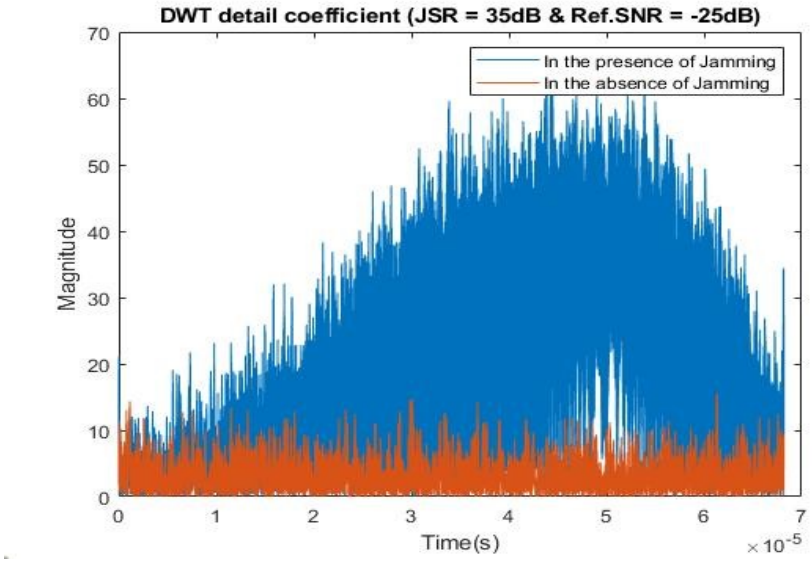

Figure 51. Comparison of selected detail coefficient in the presence of single tone chirp jammer and in the absence of jamming for JSR = 35dB.

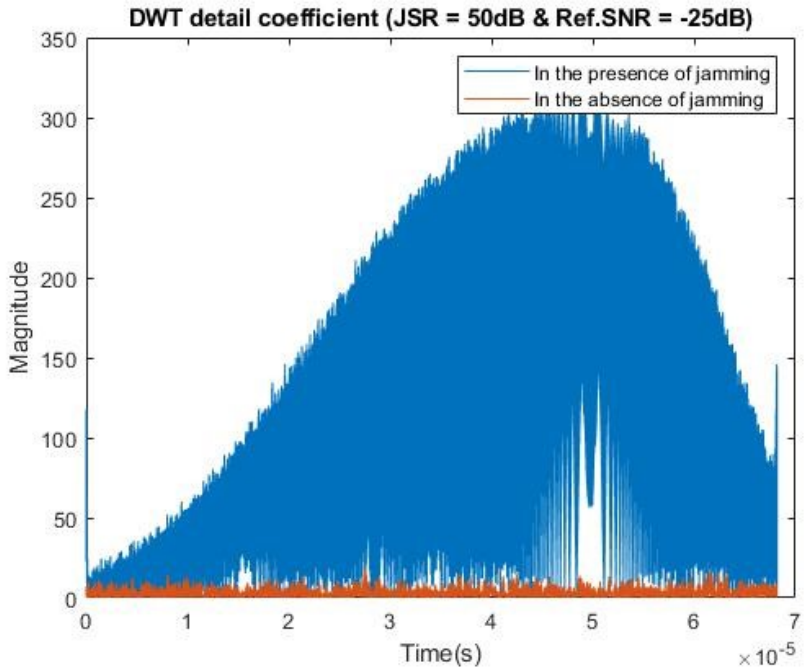

Figure 52. Comparison of selected detail coefficient in the presence of single tone chirp jammer and in the absence of jamming for JSR = 50dB.

Inference from figures 51 & 52: Higher the value of JSR, higher the strength of the jamming signal compared to noise, thereby making distinction and detection more efficient. The curved blue plot indicates the presence of a signal with certain bandwidth.

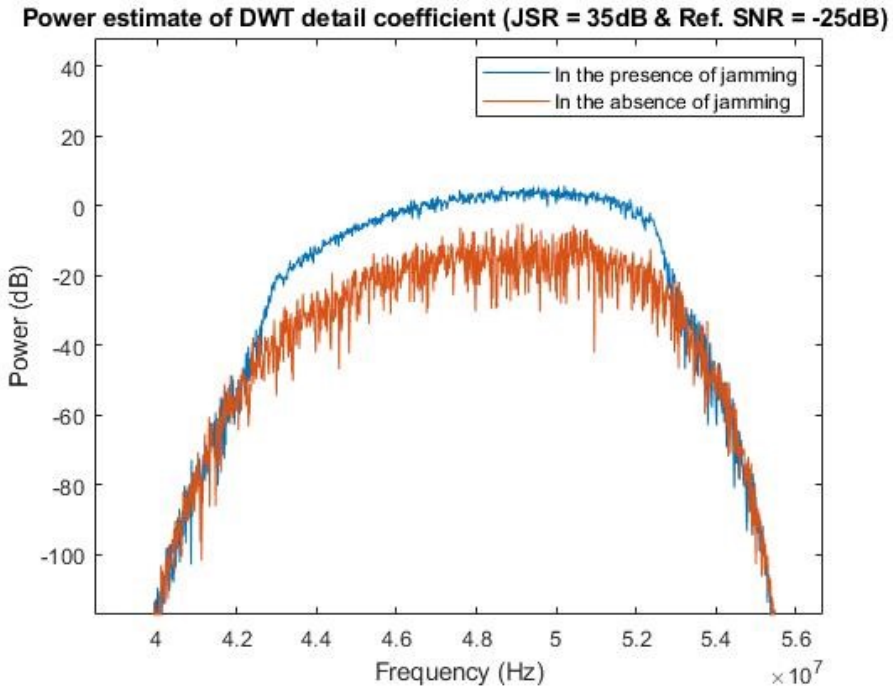

Figure 53. Power estimate comparison of the selected detail coefficient in the presence of single tone chirp jammer and in the absence of jamming for JSR = 35dB.

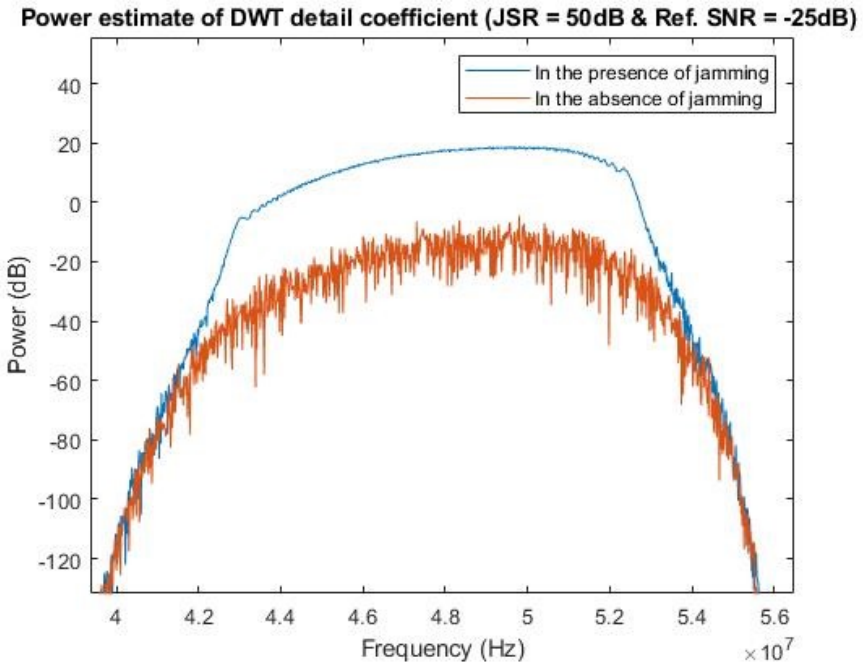

Figure 54. Power estimate comparison of the selected detail coefficient in the presence of single tone chirp jammer and in the absence of jamming for JSR = 50dB.

Inference from figures 53 & 54: Higher the value of JSR, higher is the power of the jamming signal resulting in efficient detection. High power levels can be seen from 42.7MHz to 52.7MHz which indicates the presence of jamming.

Simulation 7:

In the absence of jamming, wavelet used: Sym8 & Ref. SNR = -25dB.

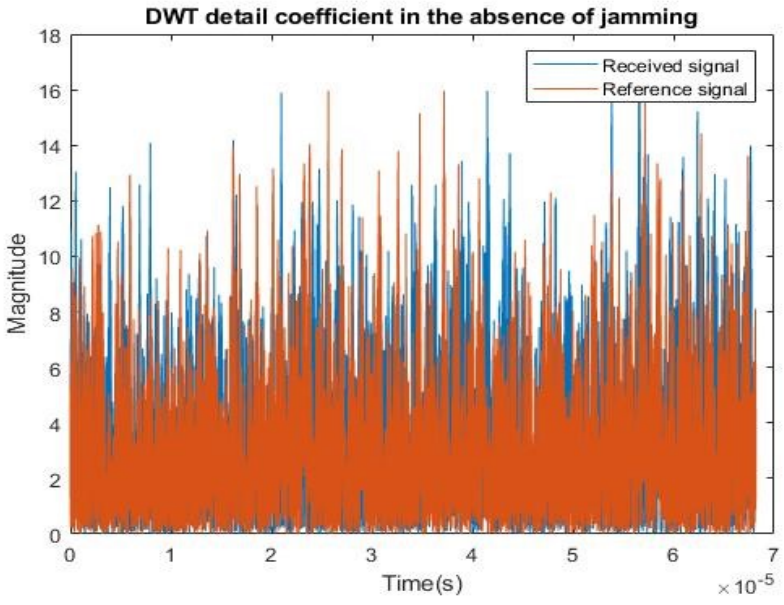

Figure 55. Comparison of selected detail coefficient of the received signal and the reference signal in the absence of jamming.

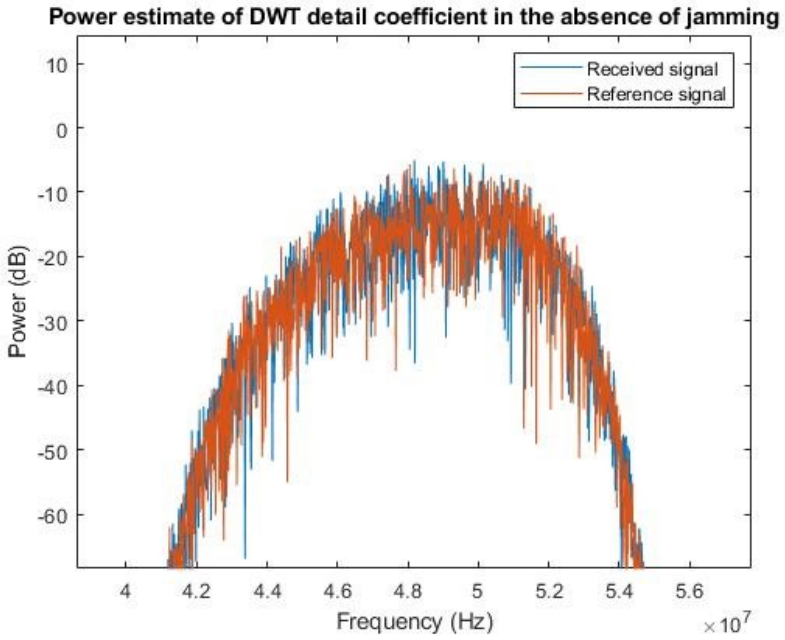

Figure 56. Power estimate comparison of the selected detail coefficient of the received signal and the reference signal in the absence of jamming.

Inference from figures 55 & 56: In the absence of jamming, the received signal and the reference signal are very similar (seen as overlaps in figures 55 and 56).

Simulation 8:

Jamming signal type: *Class 2 dual tone chirp with 10MHz (from 42.7MHz to 52.7MHz centred at 47.7MHz) and 6MHz (from 54.7MHz to 60.7MHz centred at 57.7MHz) band-width & a jamming signal with multiple frequency bursts at and around 47.7MHz,* Ref. SNR = *-25dB,* Wavelet used: *Sym8*.

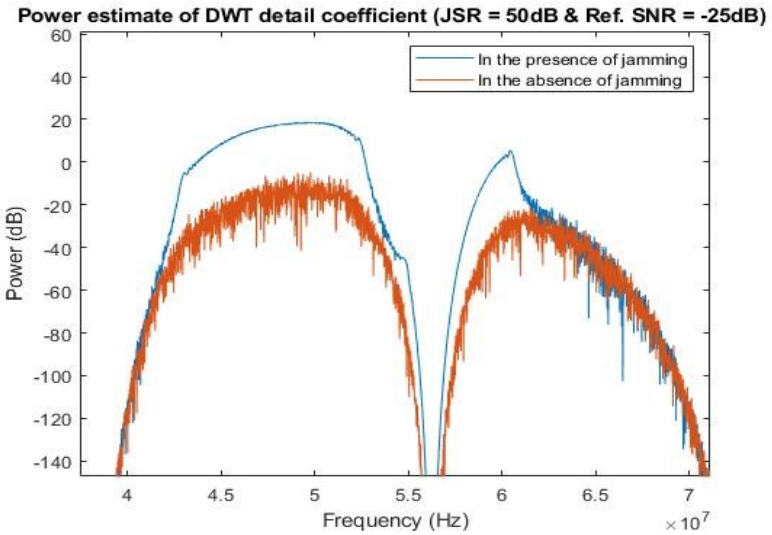

Figure 57. Power estimate comparison of the selected detail coefficient in the presence of dual tone chirp jammer and in the absence of jamming for JSR = 50dB.

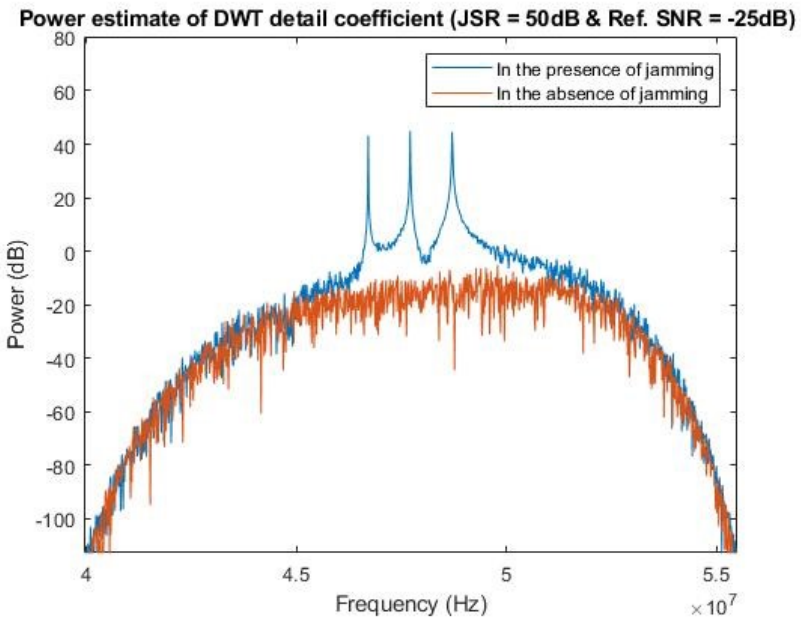

Figure 58. Power estimate comparison of the selected detail coefficient in the presence of jamming signal with multiple frequency bursts and in the absence of jamming for JSR = 50dB.

From the simulations and analysis presented so far, it is evident that the detector conceived in this thesis works efficiently in scenarios where the strength of the jamming signal is high compared to that of noise.

The operational efficiency of the detection algorithm is assessed with the help of two parameters namely, detection probability (Pd) and false alarm probability (Pfa).

3.3 Detection Probability (Pd)

Pd is the significant parameter used to judge the functionality of the detector in the presence of jamming and it depends primarily on the detection threshold T. In this study, 'T' is selected such that,

- The strength of the jamming signal is high enough compared to noise variance which enables the detector to faithfully identify any unwanted jamming components.
- The Pfa is as low as possible.

Apart from these factors, the other factors that influenced the choice of 'T' are,

- The nature of the decision metric D (how D is defined).
- The range of SNR at the front end of the GNSS receiver tuned to L1 band which is -21dB to -29dB [10].

Considering all these factors, the value of the detection threshold selected is **T = 0.45**

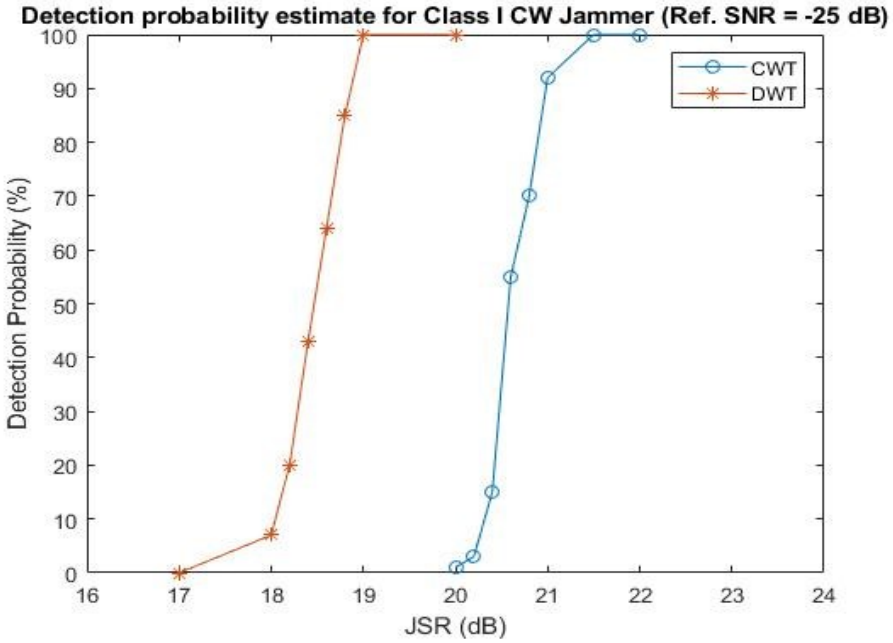

Figure 59. Detection probability estimate comparison between CWT and DWT based algorithms for class I CW jammer (Ref. SNR = -25dB).

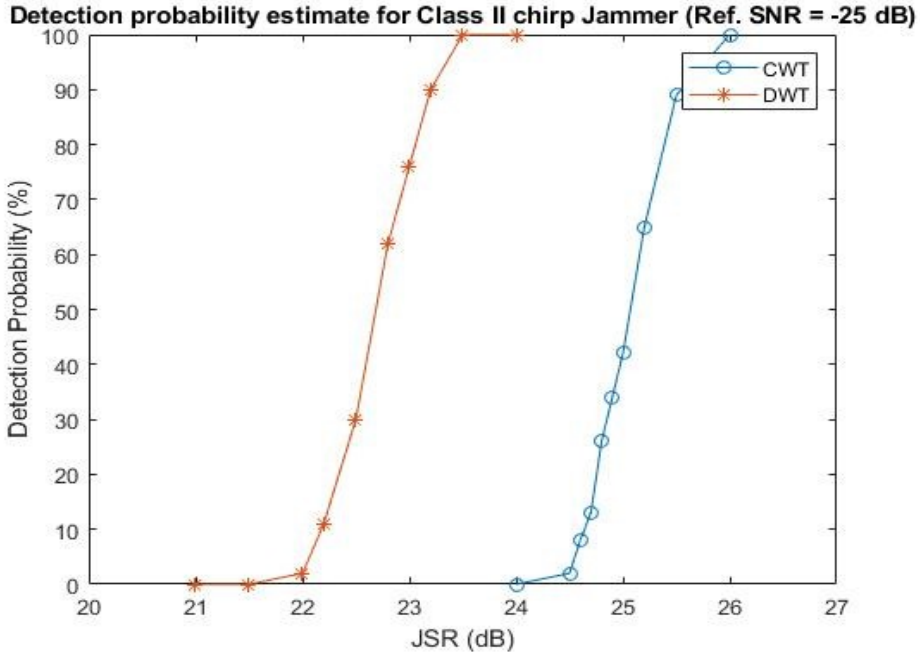

Figure 60. Detection probability estimate comparison between CWT and DWT based algorithms for class II chirp jammer (Ref. SNR = -25dB).

Inference from figures 59 & 60: In case of CWT, the detector performs efficiently in scenarios where the strength of the jamming signal is comparable to or greater than noise strength. But in case of DWT, the detector can perform well even if the jamming

signal strength is slightly weaker compared to noise. This makes the detector based on DWT better than the one based on CWT.

Type of jamming signals used in the Pd estimate simulated above are,

- Class II single tone chirp jammer with bandwidth 10MHz (42.7MHz to 52.7MHz centred at 47.7MHz) & Class I CW jammer at 47.7MHz.

Also, the IF of the down converted received GNSS signal is 47.7MHz.

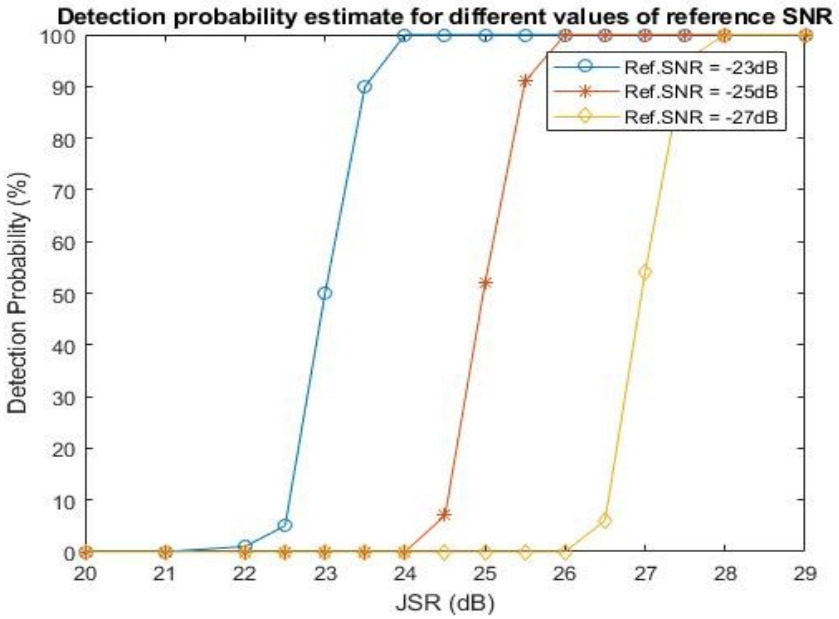

Figure 61. CWT based detection probability estimates for distinct values of reference SNR.

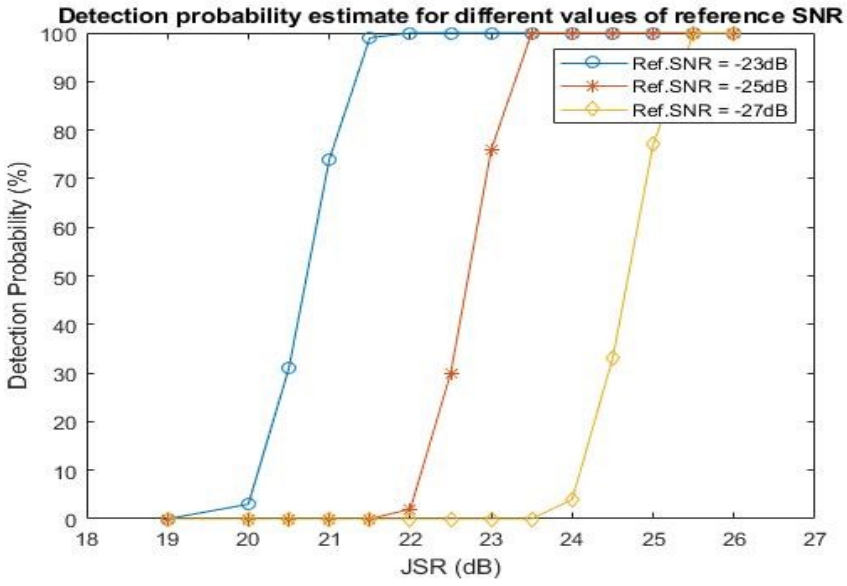

Figure 62. DWT based detection probability estimates for distinct values of reference SNR.

Figures 61 & 62 describes the functional performance of CWT and DWT based detectors respectively, under different reference SNR scenarios.

Class II single tone chirp jammer with 10MHz bandwidth (42.7MHz to 52.7MHz centred at 47.7MHz) is used in the Pd estimate for distinct reference SNRs.

The Pd estimate simulations described above reiterates the point made earlier that the detector works better, if the strength of the jamming signal is high compared to that of noise. Also, detection algorithm based on DWT performs slightly better compared to the one based on CWT under similar conditions.

In this study, the detection algorithm is based on the assumption that the source of interference is unknown meaning, interference is random. The Pd simulations described above just gives an idea on the functional behaviour of the detector in the presence of different types of jamming. The detector simulated in this study can be used to identify any types of jamming signals whether simple or complex.

3.4. False alarm probability (Pfa)

Pfa is the significant parameter used to judge the functionality of the detector in the absence of jamming. Like Pd, Pfa also depends on the detection threshold ‘T’.

Based on the chosen detection threshold T and the nature of decision metric D, the maximum Pfa estimate for,

- CWT based algorithm is 10%.
- DWT based algorithm is 9.2%.

Maximum Pfa is observed when Pd is maximum. As already mentioned Pfa depends on how the decision metric D is defined and the choice of threshold T.

- If ‘T’ is too small, maximum Pfa can be further reduced but results in rise of probability of miss in detection (1 - Pd).
- If ‘T’ is too high, probability of miss in detection (1 - Pd) will be substantially reduced but results in significant rise in maximum Pfa.

So, it is important exercise caution when selecting the decision threshold without compromising other related factors.

Suppose if we assume that the SNR range (-21dB to -29dB) [10] at the front end of the GNSS receiver tuned to L1 band is unknown. In that case the only way to make sure that Pfa is as low as possible is by manipulating the decision threshold T only, which in turn depends on the definition of decision matric D.

In this study under such circumstances, Pfa can be maintained at lower values by reducing the decision threshold T which may increase the probability of miss in detection.

The entire detection process can be mathematically modelled as [5],

- H0 = r(t) + n(t)
- H1 = r(t) + n(t) + j(t)

Where, r(t) = GNSS information signal, n(t) = noise & j(t) = jamming signal.

If D <= T, then H1 is chosen and If D > T, then H0 is chosen.

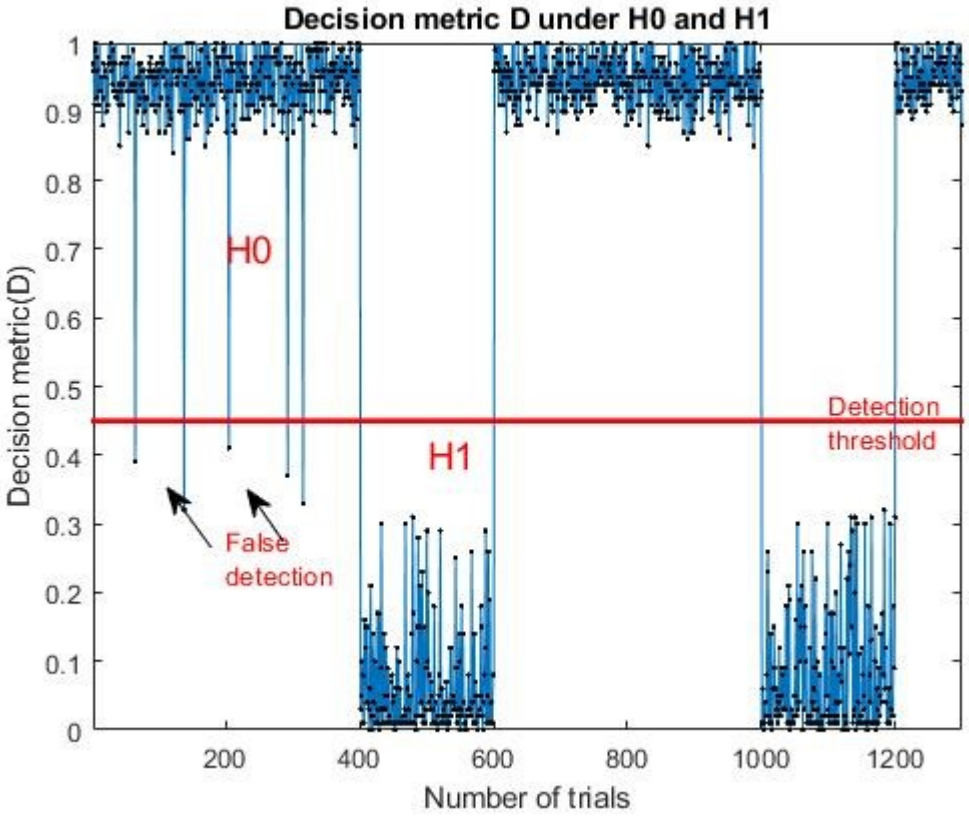

Figure 63. Decision metric (D) under H0 and H1.

Figure 63 describes the functionality of the detector in the absence of jamming (H0) and in the presence of jamming (H1).

4. CONCLUSION

GNSS satellite systems play pivotal role in modern navigation and positioning application ranging from civilian aircraft navigation to missile guidance and tracking systems. In the presence of jamming signals one can make an educated guess about the effects it has on such sensitive systems. So, it is important to understand and minimize the effect of these unwanted signals.

As they say, to eliminate a problem we need to thoroughly understand it first. The understanding part, in simple words detection is where the focus of this thesis resides. In this thesis, the detection algorithm based on the concept of wavelet transform technique is presented. From the simulation results, we can conclude that the proposed technique works efficiently in detecting wide variety of jamming signals. It also helps to capture certain important information related to jamming signals which helps to understand their nature better. The proposed detector yields reliable results in scenarios where the strength of the jamming signals is higher than the strength of noise.

Although the proposed technique has strong potential in achieving the intended objective, it offers plenty of room for improvement mainly in identification of weak jamming signals in high noise environment.

Finally, the detection technique presented in this thesis can be used as the basis (essence) for further research areas related but not restricted to jamming mitigation and practical realization aspects of the detection technique.

REFERENCES

[1] D. Borio, F. Dovis, H. Kuusniemi and L. Lo Presti, “Impact and Detection of GNSS Jammers on Consumer Grade Satellite Navigation Receivers”, IEEE proceedings Vol. 104, No. 6, June 2016.

[2] Ho-Lung Hung and Chieh-tsung Chi, “Electromagnetic Interference Detection using Wavelet Transform”, IEEE proceedings 2001.

[3] I. Daubechies, *Ten Lectures on Wavelets*, SIAM, Philadelphia, 1992.

[4] I. Daubechies, “The Wavelet Transform, Time-Frequency Localization and Signal Analysis”, IEEE Transactions on Information Theory, Vol. 36, No. 5, September 1990.

[5] B. Montella and L. Lo Presti, “Methods of Goodness of Fit for GNSS Interference Detection”, IEEE Transactions on Aerospace and Electronic Systems, Vol. 50, No. 3, July 2014.

[6] T. Krauss, R. Bauemfeind and B. Eissfeller, “Survey of In-Car Jammers – Analysis and Modelling of the RF signals and IF samples”, 24th International Technical Meeting of the Satellite Division of The Institute of Navigation, Portland, OR, September 19-23, 2011.

[7] L. Musumeci and F. Dovis, “Use of the Wavelet Transform for Interference Detection and Mitigation in Global Navigation Satellite Systems”, Research article, International Journal of Navigation and Observation, Hindawi Publishing Corporation, Vol. 2014, article ID. 262186.

[8] M. Misiti, Y. Misiti, G. Oppenheim, J.M. Poggi, MATLAB v2018b Wavelet Toolbox User’s Guide, The Mathworks Inc.

[9] Understanding Wavelets, MATLAB Youtube official tutorial Channel.

[10] Inside GNSS Magazine, “https://Insidegnss.com/”, Gibbons Media and Research LLC, Oregon, USA.

[11] Navipedia, European Space Agency Initiative, “https://gssc.esa.int/navipedia/index.php/Main_Page”.

[12] K. Borre, D.M. Akos, N. Bertelsen, P. Rinder and S.H. Jensen, *A Software Defined GPS and Galileo Receiver – A Single Frequency Approach*, Birkhauser Boston, 2007.

[13] S.L. Marple, “Time-Frequency Signal Analysis: issues and alternate methods”, Proceedings of the IEEE-SP International Symposium on Time-Frequency and Time-Scale Analysis, 1998, Pittsburgh, PA, USA.

[14] M. Medley, G.J. Saulnier and P. Das, “Radiometric Detection of Direct-Sequence Spread Spectrum Signals with Interference Excision using the Wavelet Transform”, IEEE Proceedings, 1994.

[15] E. Elsehely and M.I. Sobhy, “Reduction of Interference in Automotive radars using Multiscale Wavelet Transform”, IEEE Proceedings, 2001.

[16] J.J. Perez-Solano, S. Felici-castell and M.A/ Rodriguez-Hernandez, “Narrowband Interference Suppression in Frequency Hopping Spread Spectrum using Undecimated Wavelet Packet Transform”, IEEE Transactions on vehicular technology, Vol. 57, No. 3, May 2008.

[17] W. Qu, X. Jia and S.L.Y. Wu, “SAR Interference Signal Feature Extraction and Simulation based on Wavelet Packet Analysis”, IEEE EMB, 3rd International congress on image and Signal processing, 2010.

[18] G.F. Forte, J.M. Tarongi and A. Camps,” Hardware Implementation of wavelet-based Radio Frequency interference Mitigation Algorithm for Microwave Radiometers”, IEEE Proceedings 2011, IGARSS 2011.

[19] S. Abbaspour, A. Fallah, M. Linden and H. Gholamhosseni, “A novel approach for removing ECG interferences from surface EMG signals using a combined ANFIS and Wavelet”, Journal of Electromyography and Kinesiology, 2015 Elsevier Ltd. Available at ScienceDirect.

[20] F. Zhang and M. Li, “Wavelet Analysis method of harmonics and electromagnetic interference in coal mines”, Mining Science and Technology, 2010 Elsevier Ltd. Available at ScienceDirect.

[21] F. Bastide, D. Akos, C. Macabiau and B. Roturier, “Automatic Gain Control (AGC) as an interference assessment tool”, Proceedings of the ION GPS 2003, Portland, Oregon, USA.

[22] B. Montella, M. Pini and F. Dovis, “Investigation on the effect of strong out- of-band signals in GNSS Receivers”, GPS Solutions, 12, 2(2008), 77-86

[23] P.F.D. Bakker, J. Samson, M. Spelat, M. Hoolreiser and B. Ambrosius, “Effect of radio frequency interference on GNSS receiver output”, Proceedings of the ESA workshop on Satellite Navigation User Equipment Technologies NAVITEC, Noordwijk, Netherlands, 2006.

[24] S. Pullen and G.X. Gao, “GNSS jamming in the name of privacy”, Inside GNSS, (Mar/Apr. 2012), 34-43.

[25] L. Marti and F. Van Graas, “Interference detection by means of the software defined radio”, ION GNSS 17th International Meeting of the Satellite Division, Long Beach, CA, 2004.

[26] A. Balaei and A. Dempster, “A statistical inference technique for GPS interference detection”, IEEE Transactions on Aerospace and Electronic Systems, 45, 4 (October 2009).

[27] M.L. Rizzo, “New goodness-of-fit tests for Pareto distributions”, ASTIN Bulletin: Journal of the International Association of Actuaries, 39, 2 (Nov.2009).

[28] S.M. Kay, “Fundamentals of Statistical Signal Processing Detection Theory (Vol.2)”, Prentice Hall, 1993, New Jersey.

[29] S.S. Wilks, “Mathematical Statistics”, John Wiley & Sons Inc. 1962.

[30] M. Jones, “The Civilian Battlefield – Protecting GNSS Receivers from Interference and jamming”, Inside GNSS, March/April 2011.

[31] E.D. Kaplan and C.J. Hegarty, “Understanding GPS Principles and Applications”, Artech House, 2006, USA.

[32] D. Borio, “GNSS acquisition in the presence of continuous wave interference”, IEEE Transactions on Aerospace and Electronic Systems, vol. 46, no.1, 2010.

[33] S. Savasta, L.L. Presti and M. Rao, “Interference mitigation in GNSS receivers by a time-frequency approach”, IEEE Transaction on Aerospace and Electronic Systems, Vol. 49, no. 1, January 2013.

[34] S.G. Mallat, “Theory for multiresolution signal decomposition: the wavelet representation”, IEEE Transactions on Pattern Analysis and Machine Intelligence, vol. 11, no. 7, 1989.

[35] Ho-Lung, Hung, Jyh-Ching, Yang, “An effect approach for EMI problems via wavelet techniques”, Proceeding of the 20th Symposium on Electrical Power Engineering, Nov. 1999.